

THE STAR FORMATION AND NUCLEAR ACCRETION HISTORIES OF NORMAL GALAXIES
IN THE AGES SURVEY

CASEY R. WATSON¹, CHRISTOPHER S. KOCHANEK², WILLIAM R. FORMAN³, RYAN C. HICKOX³,
CHRISTINE J. JONES³, MICHAEL J. I. BROWN⁴, KATE BRAND⁵, ARJUN DEY⁶, BUELL T.
JANNUZI⁶, ALMUS T. KENTER³, STEVE S. MURRAY³, ALEXEY VIKHLININ³, DANIEL J.
EISENSTEIN⁷, GIOVANI G. FAZIO³, PAUL J. GREEN³, BRIAN R. MCNAMARA⁸, MARCIA RIEKE⁶,
JOSEPH C. SHIELDS⁸

ABSTRACT

We combine IR, optical and X-ray data from the overlapping, 9.3 deg² NOAO Deep Wide-Field Survey (NDWFS), AGN and Galaxy Evolution Survey (AGES), and XBoötes Survey to measure the X-ray evolution of 6146 normal galaxies as a function of absolute optical luminosity, redshift, and spectral type over the largely unexplored redshift range $0.1 \lesssim z \lesssim 0.5$. Because only the closest or brightest of the galaxies are individually detected in X-rays, we use a stacking analysis to determine the mean properties of the sample. Our results suggest that X-ray emission from spectroscopically late-type galaxies is dominated by star formation, while that from early-type galaxies is dominated by a combination of hot gas and active galactic nucleus (AGN) emission. We find that the mean star formation and supermassive black hole accretion rate densities evolve like $\sim (1+z)^{3\pm 1}$, in agreement with the trends found for samples of bright, individually detectable starburst galaxies and AGN. Our work also corroborates the results of many previous stacking analyses of faint source populations, with improved statistics.

Subject headings: cosmology: observations — galaxy evolution

1. INTRODUCTION

There are three primary sources of galactic X-ray emission: diffuse, hot gas, accreting stellar remnants, such as X-ray binaries, and accreting supermassive black holes (SMBHs), i.e., active galactic nuclei (AGNs). Apart from nearby ellipticals, which tend to be dominated by hot gas emission (e.g., Forman, Jones, & Tucker 1994), local surveys indicate that X-ray binaries dominate the flux from “normal” galaxies with quiescent nuclei (e.g., Fabbiano & White 2003, Smith & Wilson 2003, Munro et al. 2004). There are two distinct populations of X-ray binaries: the short-lived ($\lesssim 10^6$ yr), high-mass X-ray binaries (HMXBs) and the long-lived ($\gtrsim 10^8$ yr), low-mass X-ray binaries (LMXBs). Because of their short lifetimes, one expects the X-ray emission from HMXBs to track the current star formation rate (SFR). In contrast, the X-ray emission from longer lived LMXBs should track the integrated stellar mass with some time lag due to stellar and binary evolution (e.g., Ghosh & White 2001, Ptak et al. 2001, Grimm et al. 2003).

These expectations are largely borne out by observations. There are strong correlations between the hard

(> 2 keV) X-ray luminosity (presumably from HMXBs) and other star formation indicators, such as radio, far-IR, *B*-band, and UV flux for both local (e.g., Fabbiano 1989, David, Jones, & Forman 1992) and higher redshift (Seibert et al. 2002, Bauer et al. 2002) galaxy samples. Many studies have found a linear correlation between X-ray luminosity and the SFR (e.g., Ranalli et al. 2003, Grimm et al. 2003, Gilfanov et al. 2004, Persic et al. 2004; Colbert et al. 2004). In particular, Grimm et al. (2003) found that the hard (2–10 keV) HMXB X-ray luminosity scales with the SFR according to

$$L_{x,\text{hard}}^{\text{HMXB}} \simeq 0.67 \times 10^{40} \left(\frac{\text{SFR}}{M_{\odot}\text{yr}^{-1}} \right) \text{ ergs s}^{-1}. \quad (1)$$

In contrast, the (total band: 0.5–8 keV) X-ray emission from LMXBs is well correlated with the *K*-band flux of galaxies, which in turn is a good tracer of stellar mass. Kim and Fabbiano (2004) find that

$$L_x^{\text{LMXB}} \simeq 10^{40} \left(\frac{L_K}{L_{K*}} \right) \text{ erg s}^{-1}, \quad (2)$$

where $L_{K*} = \nu_K L_{\nu_K,*} = 2.6 \times 10^{43} \text{ erg s}^{-1}$ corresponds to $M_{K*} = -23.4 \text{ mag}$ (Kochanek et al. 2001).

Because the stellar mass density evolves slowly between $z = 0$ and $z \simeq 0.5$ (e.g., Bell 2004 and references therein), we expect little change in the number of LMXBs and assume that Eqn. (2) holds out to $z \simeq 0.5$. On the other hand, the SFR density rises rapidly with look-back time, (e.g., $\propto (1+z)^{2.7\pm 0.7}$ Hogg 2001), so we should see a correspondingly rapid evolution in the X-ray flux of star-forming galaxies due to the increasing number of HMXBs.

The accretion luminosity density of AGNs also rises rapidly with redshift (e.g., $\propto (1+z)^{3.2\pm 0.8}$, Barger et al. 2005) with higher densities of more luminous sources at higher redshifts (e.g., Barger et al. 2001, Cowie et al. 2003, Ueda et al. 2003, Miyaji 2004, Hasinger 2005, Hasinger, Miyaji, & Schmidt 2005). The observed trends suggest that faint AGNs with characteristic X-ray luminosities approaching those of bright starbursts, $L_x \lesssim 10^{41} \text{ ergs s}^{-1}$,

¹ Department of Physics and Astronomy, Millikin University, 1184 West Main Street, Decatur, IL 62522; crwatson@millikin.edu

² Department of Astronomy, The Ohio State University, 140 West 18th Avenue, Columbus, OH 43210; Center for Cosmology and Astro-Particle Physics, The Ohio State University, Columbus, Ohio 43210

³ Harvard-Smithsonian Center for Astrophysics, 60 Garden Street, Cambridge, MA 02138

⁴ School of Physics, Monash University, Clayton, Victoria, 3800, Australia

⁵ Space Telescope Science Institute, 3700 San Martin Drive, Baltimore, MD 21218

⁶ National Optical Astronomy Observatory, Tucson, AZ 85726-6732

⁷ Steward Observatory, University of Arizona, 933 North Cherry Avenue, Tucson, AZ 85721

⁸ Department of Physics and Astronomy, Ohio University, Athens, OH 45701

may be most abundant at $z \lesssim 1$ and, if so, they could produce a substantial fraction of the “normal” galaxy X-ray flux at these redshifts.

Given their similar evolution, spectral shapes (e.g., Ptak et al. 1999), and potentially similar luminosities, it may be difficult to disentangle the X-ray emission from AGNs and star formation at $z \lesssim 1$. Probing the X-ray evolution of normal galaxies between $z \simeq 0.1$ and $z \simeq 1$ is also difficult because it requires relatively deep observations over relatively wide areas. In fact, most of our knowledge about the X-ray properties of galaxies still comes from either large-area, local surveys (e.g., Fabbiano 1989; David et al. 1992) or high-redshift, small-volume deep fields (e.g., Georgakakis et al. 2007; Ptak et al. 2007; Tzanavaris & Georgantopoulos 2008).

This is the second in a series of papers in which we attempt to bridge this gap by examining the X-ray evolution of galaxies within the 9.3 deg^2 Boötes field of the NOAO Deep Wide-Field Survey (NDWFS; Jannuzi & Dey 1999, B. T. Jannuzi et al., in preparation, A. Dey et al. in preparation). The XBoötes survey (Murray et al. 2005) obtained a 5 ks Chandra mosaic of the entire 9.3 deg^2 field based on 126 ACIS-I pointings. These data are too shallow, however, to detect typical galaxies even at modest redshifts. Fortunately, the wide area of the survey allows us to measure the mean properties of a large, representative population of galaxies by “stacking” (averaging) their X-ray emission (Brandt et al. 2001; Nandra et al. 2002; Hornschemeier et al. 2002, Georgakakis et al. 2003, Lehmer et al. 2005, 2007, 2008; Laird et al. 2005, 2006).

In the first paper in the series, Brand et al. (2005; hereafter B05) employed the stacking technique to examine the X-ray luminosity evolution of ≈ 3300 optically luminous ($\sim L_*$), red galaxies with photometric redshifts $0.3 < z < 0.9$. By constraining the sample to have the same evolution-corrected, absolute R -band magnitude distribution at all redshifts ($M_R < -21.3$, $\langle M_R \rangle \simeq -22.0$), it was possible to follow the nuclear accretion histories of a consistent population of galaxies throughout this epoch. Because these massive, early-type galaxies are the typical hosts of powerful quasars at higher redshifts (McLeod & McLeod 2001; Dunlop et al. 2003), tracking the decay of their nuclear activity to lower redshifts is essential to our understanding of the decline in SMBH accretion from its peak during the quasar phase ($z \gtrsim 2$) to the present. The observed variation in the nuclear accretion rate of the $> L_*$ red galaxies, $L_x \propto (1+z)^{4\pm 2.4}$, is broadly consistent with the behavior of bright, individually detected AGNs studied by Barger et al. (2001; hereafter Ba01) and Barger et al. (2005; hereafter Ba05).

In the present paper, we combine the NDWFS and XBoötes surveys with redshifts from the AGN and Galaxy Evolution Survey (AGES, C. S. Kochanek et al. 2009, in preparation) to study the X-ray properties of a complete, flux-limited sample of galaxies as a function of absolute optical luminosity, redshift, stellar mass, and spectral type. While our general procedures are similar to those of other recent stacking analyses (e.g., Brandt et al. 2001; Nandra et al. 2002; Hornschemeier et al. 2002; Georgakakis et al. 2003, Laird et al. 2005, 2006; Lehmer et al. 2007), the number of objects we consider (≈ 6500) is 10–100 times larger. The size of our sample allows us to convert the short mean

exposure time of the XBoötes survey (5 ks) into stacked, effective exposure times that are large enough to detect galaxies at intermediate redshift (Msec).

In Section 2 we describe the data and illustrate our ability to detect X-ray emission from the AGES galaxies through the stacking approach. In Section 3 we provide further details of our stacking analysis and use Monte Carlo simulations to test it and to refine our choices of signal and background apertures. In Section 4 we present measurements of the mean evolution of all the AGES galaxies. We then consider the radial emission profiles of a nearby ($z \leq 0.1$) subsample in order to test for weak/obscured AGNs. We also examine the hardness and X-ray to optical luminosity ratios as a function of redshift, stellar mass, and spectroscopic type (late-type, early-type, or AGNs). Based on these tests, we evaluate the relative contributions of hot gas, LMXBs, HMXBs, and AGNs emission to the observed signal. We then discuss our results and compare them to previous studies. Lastly, we determine the evolution of the SFR per unit galactic stellar mass and the SFR density based on emission from the late-type galaxy sample and trace the evolution of the nuclear accretion rate and accretion rate density of AGNs in the early-type galaxy sample. We summarize our findings in Section 5. Throughout the paper, we assume a flat Λ cold dark matter (Λ CDM) cosmology with $\Omega_{m,0} = 0.3$, $\Omega_{\Lambda,0} = 0.7$, and $H_0 = 70 \text{ km s}^{-1} \text{ Mpc}^{-1}$.

2. THE X-RAY DATA, THE GALAXY SAMPLE AND METHODS

The NDWFS obtained B_W , I , R , and (partial) K -band observations of two roughly 9.3 deg^2 regions. The Northern Boötes field has also been surveyed at radio (VLA FIRST, Becker et al. 1995 and WSRT, de Vries et al. 2002), far-IR (Spitzer/MIPS, Soifer et al., 2004), mid-IR (Spitzer/IRAC, The IRAC Shallow Survey, Eisenhardt et al., 2004), near-IR (NDWFS and the Flamingos Extragalactic Survey; Elston et al. 2006), UV (GALEX; Hoopes 2004), and X-ray (XBoötes, Murray et al. 2005) wavelengths. In particular, the XBoötes survey covered the entire Northern Boötes field with 126 $17' \times 17'$ ACIS-I images of mean exposure time 5 ks using the Chandra X-ray Observatory (Murray et al. 2005). The survey detected approximately 3300 point sources and 43 extended sources in the field with ≥ 4 counts (4767 sources with ≥ 2 counts, Kenter et al. 2005).

2.1. X-ray Data

For our current analysis, we use the positions of the 420,000 photons detected in the XBoötes observations, with weights correcting for off-axis vignetting and variations in exposure time, their estimated energies $\epsilon \pm \delta\epsilon$, and their positions relative to the pointing center of the observations. We limited the analysis to photons with $0.5 < \epsilon < 7 \text{ keV}$, dividing them into total (0.5–7 keV), hard (2–7 keV), and soft (0.5–2 keV) energy bands. The mean total, hard, and soft backgrounds measured during these observations were approximately 2.8, 1.9, and 0.96×10^{-3} counts arcsec $^{-2}$, respectively.

For the normal galaxies, the average ratio between the hard and soft X-ray counts is 0.73. To fit this count ratio, we assume an absorbed power-law $dN(E)/dE \propto$

$E^{-\Gamma}$ (counts s^{-1} keV $^{-1}$) for the intrinsic X-ray spectrum. We then use portable, interactive multi-mission simulator (PIMMS v3.9d)⁹ to find the best-fit photon index, $\Gamma = 1.29$, assuming a fairly low absorption column density ($N(H) = 4 \times 10^{20}$ cm $^{-2}$), half of which is the Galactic absorption for the B \ddot{o} otes field from Stark et al. (1992). Factor of 2 changes in the assumed column densities change Γ by only a few percent. The spectrum of the “normal” galaxies is very similar to that of the Cosmic X-ray Background (CXB), $\Gamma_{\text{CXB}} \simeq 1.4$ (e.g., Tozzi et al. 2001; Nandra et al. 2004) and of resolved populations in the Chandra Deep Fields (e.g., Civano, Comastri, & Brusa 2005). Photon indices in this range are also typical for both X-ray binaries and obscured AGNs ($1 \lesssim \Gamma \lesssim 2$, e.g., Ptak et al. 1999, Munro et al. 2004). Based on our model of the composite AGES galaxy X-ray spectrum, we estimate that one soft, hard or total band count corresponds to 1.05×10^{-15} erg cm $^{-2}$ s $^{-1}$, 3.65×10^{-15} erg cm $^{-2}$ s $^{-1}$ and 2.14×10^{-15} erg cm $^{-2}$ s $^{-1}$, respectively, for an on-axis source with a 5 ks exposure time.

2.2. The Galaxy Sample

For our stacking analysis, we cross referenced the XBo \ddot{o} tes catalog of X-ray photon positions (i.e., the event list) with those of the galaxies observed by the AGES (C. S. Kochanek et al. 2009, in preparation). We focus on the approximately 6500 galaxies in the 2004 AGES main galaxy sample. This sample consists of all galaxies with $R < 19.2$ mag and a randomly selected 20% of galaxies with $19.2 < R < 20$ mag. We use Vega magnitudes throughout the paper. The spectroscopic redshifts of the galaxies were measured using Hectospec, a robotic 300 fiber spectrograph for the MMT (Fabricant et al. 1998, Roll et al. 1998, Fabricant et al. 2005) and are 95% complete for $R < 19.2$; our analysis is not significantly affected by the modest level of incompleteness. Although we have redshifts for roughly half of the remaining 80% of galaxies with $19.2 < R < 20$ mag, we do not include them in this analysis because they were not targeted based on a simple R -band flux-limited criterion.

Redshifts were measured using two independent data reduction pipelines (the Hectospec pipeline at the CfA and a modified SDSS pipeline at Steward Observatory), and the results were verified by visually inspecting the spectra for features consistent with the pipeline redshift. Both the pipelines and the visual inspection flagged galaxies with spectroscopic signatures of AGNs, both obvious broad-lined systems and those with emission-line ratios characteristic of Type II optical AGNs. We also carried out a principal component analysis of the optical spectra (e.g., Formigini & Brosch 2004, Ferreras et al. 2006). In our analysis, the level of star formation was largely characterized by the ratio of the second component relative to the first, so we divided the sample into early and late-type galaxies at the median of the distribution of that ratio for the full AGES galaxy sample.

Rest-frame absolute R -band magnitudes, M_R , were determined by combining the redshift measurements with the standard Λ CDM cosmology and the `kcorrect` algorithm (Blanton et al. 2003) adapted to the AGES data and the NDWFS B_W , I , and R photometric filters. Figure 1 shows the distribution of the galaxies as a function

of redshift and absolute magnitude. The median redshift of the galaxies is $\langle z \rangle \simeq 0.25$ with an appreciable tail extending to $z \approx 0.6$. The change in the density of points at fainter magnitudes is due to the random 20% sampling of the fainter galaxies. To compensate for this effect, we weight the emission from these galaxies by a factor of 5.

We also determined the rest-frame K -band luminosities, L_K , with `kcorrect`. We use the K -band luminosities to estimate the contribution of LMXBs to the observed X-ray emission (Eqn. 2), and to estimate the stellar mass

$$M_* \simeq (8.0 \pm 2.0) \times 10^{10} \left(\frac{L_K}{L_{K*}} \right) M_\odot, \quad (3)$$

based on the results of Colbert et al. (2004, also see Gilfanov 2004). To explore how late-type galaxies of different masses contribute to star formation, we then combine our estimates of the stellar mass and the SFR (determined using Eqn. 1) to compute the specific star formation rate (SSFR) = SFR/ M_* (e.g., Cowie et al. 1996, Guzman et al. 1997, Brinchmann & Ellis 2000, Juneau et al. 2005, Feulner et al. 2004, P \acute{e} rez-Gonz \acute{a} lez et al. 2005).

If, instead of star formation, the X-ray emission is primarily due to accretion onto AGNs, then we can estimate the SMBH growth rates, \dot{M}_{BH} , using the scaling of Ba01,

$$\dot{M}_{\text{BH}} = 1.76 \times 10^{-6} \left(\frac{\epsilon}{0.1} \right)^{-1} L_{x40}^{\text{AGN}} M_\odot \text{yr}^{-1}, \quad (4)$$

where L_{x40}^{AGN} is the AGN luminosity in units of 10^{40} erg s $^{-1}$ and ϵ is the efficiency of energy conversion in AGNs. Cowie et al. (2003) and Ba05 showed that the X-ray luminosities of both obscured and unobscured AGNs (with 10^{42} erg s $^{-1} < L_x < 10^{44}$ erg s $^{-1}$) are consistent with a radiative efficiency of $\epsilon \simeq 0.1$ all the way to $z = 0$. Moreover, the results of AGN models do not agree with observations if one assumes that lower radiative efficiency AGNs dominate black hole growth (e.g., Shankar et al. 2004, Hopkins et al. 2007). We will therefore adopt $\epsilon = 0.1$ throughout the paper.

To fit the X-ray luminosities of the AGES galaxies as a function of K -band luminosity and redshift, we assume

$$L_x \propto L_K^\alpha (1+z)^\beta. \quad (5)$$

In order to estimate the mean star formation density $\dot{\rho}_*$ and nuclear accretion rate density $\dot{\rho}_{\text{BH}}$ we must extrapolate our results from the magnitude-limited AGES galaxy samples to fainter fluxes. By assuming our power-law model (Eqn. 5) holds for fainter sources and combining the K -band luminosity functions for late- and early-type galaxies measured by Kochanek et al. (2001), with a change of variables from L_K to L_x , we compute the X-ray luminosity density as a function of redshift. The X-ray luminosity density can then be converted to star formation or nuclear accretion rate densities using Eqns. (1) or (4), respectively.

We restrict our analysis to a sample of 6146 “normal” galaxies with no optical or X-ray evidence of AGN activity. When stacked, these galaxies produce a total of 486/669 hard/soft counts above the background level. In Table 1, we compare the emission from the normal galaxies to two classes of sources we exclude from the analysis. We eliminated 47 spectroscopically identified AGNs (3 broad line and 44 narrow line) that were *not* identified in the XBo \ddot{o} tes Survey (Kenter et al. 2005), but these produced

⁹ <http://heasarc.nasa.gov/Tools/w3pimms.html>

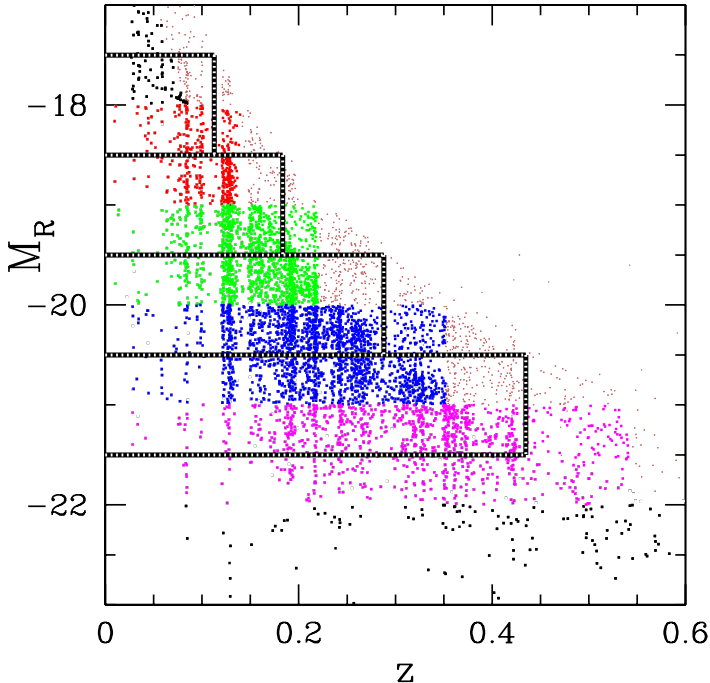


FIG. 1.— Absolute R -band magnitudes of the AGES main sample of galaxies as a function of redshift. The transition from higher to lower density background points reflects differences in sampling: all $R < 19.2$ galaxies are present but only a random 20% of galaxies with $19.2 < R < 20$ have been sampled. Four of the eight absolute magnitude strips of galaxies we analyze are outlined.

a stacked flux of only 32/27 hard/soft counts. Much more importantly, we excluded 58 galaxies that were identified both by XBöotes as X-ray sources and by AGES as spectroscopic broad line (24) or narrow line (34) AGNs. Although these 58 AGNs represent less than 1% of our sample by number, they generate 787/1196 hard/soft counts – nearly twice the X-ray flux of the normal galaxies – and would therefore dominate our results if they were not eliminated from the analysis (see Figure 5). Note, however, how similar the composite X-ray spectrum of the remaining “normal” galaxies ($\Gamma_{\text{Normal}} \simeq 1.3$) is to that of these AGNs ($\Gamma_{\text{AGN}} \simeq 1.3$) and to that of typical AGNs, which account for the bulk of Cosmic X-ray Background (CXB; $\Gamma_{\text{CXB}} \simeq 1.4$, e.g., Tozzi et al. 2001; Nandra et al. 2004). The remaining “normal” galaxies therefore provide a representative sampling of the CXB source population, and, in fact, comprise $\approx 8.8\%$ of the total CXB emission, based on the soft and hard band CXB flux estimates of De Luca & Molendi (2004).

3. METHOD, MONTE CARLO SIMULATIONS AND TESTS

The basic principle of a stacking analysis is simple. The X-ray images of a large number of sources are stacked to determine the mean properties of a group of objects that are individually undetectable (Brandt et al. 2001; Nandra et al. 2002; Hornschemeier et al. 2002, Georgakakis et al. 2003, Lehmer et al. 2005, 2007; Laird et al. 2005, 2006). Quantitatively, if stacking a sample of n objects yields N_s counts in a signal aperture of area A_s and N_b counts in a background annulus of area A_b , then the mean number of

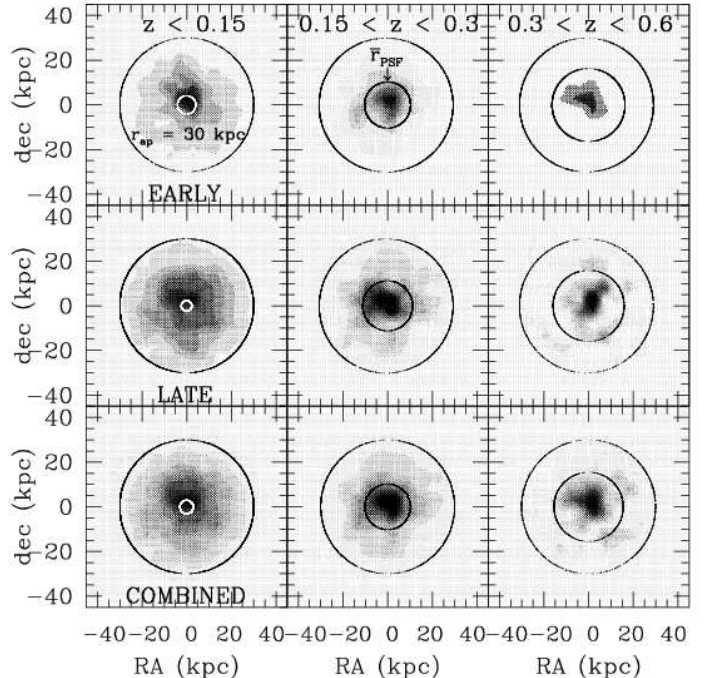


FIG. 2.— Total band X-ray images of the stacked early-type, late-type, and combined samples of galaxies have been Gaussian smoothed on a scale of 5 kpc and divided into three redshift bins: $0 < z < 0.15$, $0.15 < z < 0.3$, and $0.3 < z < 0.6$. We have included only galaxies (extended sources) that had no obvious optical signatures of AGN activity. In each panel, the outer circle shows the fixed 30 kpc aperture we use to extract the signal and the inner circle shows the size of the 50% enclosed energy radius averaged over the field and converted to a physical scale based on the mean redshift of each bin ($\bar{r}_{\text{PSF}} \simeq 2, 10, \text{ and } 15$ kpc, respectively).

source counts per object in the signal region is

$$\langle N \rangle_{\text{src}} = \frac{1}{n} \left[N_s - \frac{A_s}{A_b} N_b \right]. \quad (6)$$

The uncertainties in $\langle N \rangle_{\text{src}}$ can be computed either by assuming a Poisson distribution of X-ray counts per object,

$$\sigma = \frac{1}{n} \left[N_s + \frac{A_s^2}{A_b^2} N_b \right]^{1/2}, \quad (7)$$

or by bootstrap resampling of both the galaxy and X-ray photon catalogs (event lists). Adopting the latter method, we generate 100 bootstrap samples by randomly drawing new lists of galaxies and X-ray photons (with replacement) from the input catalogs until each bootstrap sample contains the same number of galaxies and X-ray photons as the real catalogs. Each mock data set is then subjected to the same analysis as the real data. Our error estimates are defined by the range encompassing 68% of the bootstrap results about the true mean. This approach will produce more realistic error bars than the Poisson statistics of the stacked image, particularly if the net flux is dominated by a small fraction of the objects included in the analysis.

As a general proof of principle for the subsequent analyses, Figure 2 shows images of the stacked early-type, late-type and combined samples of galaxies in three redshift bins, excluding direct X-ray detections and galaxies with optical signatures of AGN activity. Based on the Monte Carlo simulations we discuss in the following section, we

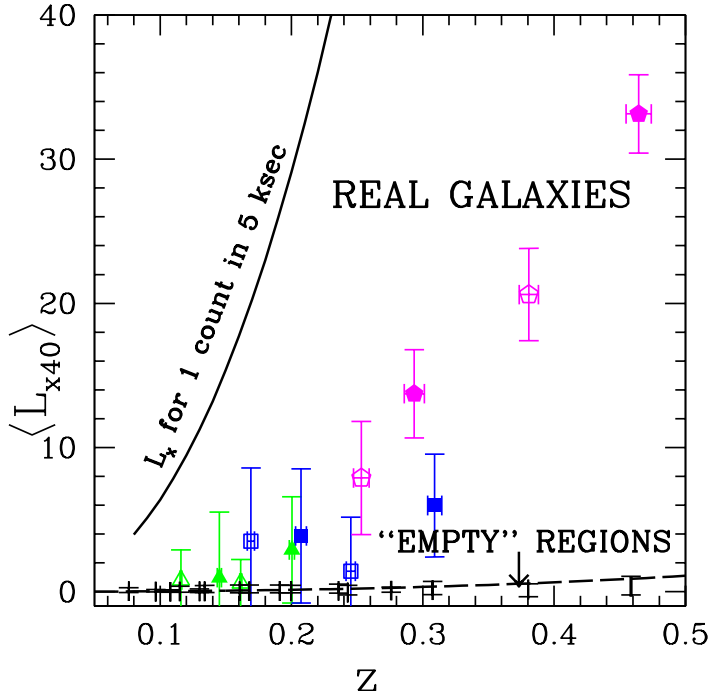


FIG. 3.— Comparison of the mean X-ray luminosities of the AGES normal galaxies and of random locations in the XBoötes field. The mean X-ray luminosities (in units of $10^{40} \text{ erg s}^{-1}$) of galaxies drawn from bins in the half-integer (integer) absolute magnitude strips with $M_R < -19$ (see Figure 1) are designated, from faint to bright, by open (closed) triangles, squares and pentagons. No statistically significant X-ray flux was detected from the intrinsically faintest galaxies. Most of the trend here is due to the higher redshifts of the more massive (and luminous) galaxies in our flux-limited sample. The dashed line shows our expected sensitivity limit given the 5 ks exposure time and the typical number of objects in each bin (see Section 3). Note that through stacking we are able to detect average X-ray signals that are much less than the luminosity equivalent of one total band count (solid line).

adopt a 30 kpc signal aperture and a 30–60 kpc background annulus about the center of each galaxy. Each panel shows this signal aperture and the field-averaged point-spread function (PSF), i.e., the 50% enclosed energy radius averaged over the field and converted to a physical scale based on the mean redshift of each bin. We clearly detect a signal from these “normal” galaxies.

To understand the X-ray evolution of the galaxies quantitatively, we bin them by absolute magnitude, spectroscopic type and redshift. We analyze the galaxies in staggered, 1 mag wide absolute magnitude strips (see Figure 1), beginning at integer and half-integer absolute magnitudes (i.e., $-17.5 > M_R > -18.5$, $-18 > M_R > -19$, $-18.5 > M_R > -19.5$, . . . $-20 > M_R > -21$). We divide each strip into two redshift bins that contain roughly equal numbers of galaxies after correcting for the sparse sampling. We also analyze the combined, late-type, and early-type galaxy samples separately. For each bin we then determine the mean X-ray and rest-frame K -band luminosities of the member galaxies. Because the X-ray and optical luminosities of galaxies are approximately linearly correlated (e.g., David, Jones, & Forman 1992; Shapley et al. 2001), the X-ray to optical luminosity ratio should provide a measure of the redshift evolution of normal galaxy

X-ray emission that is essentially independent of galaxy (optical) luminosity and stellar mass (Eqn. 3).

In addition to spectroscopically identified AGNs, we excluded directly detected X-ray sources that did not satisfy

$$L_x \leq 6.6 \times 10^{42} \text{ erg s}^{-1} \text{ (luminosity limit),} \quad (8)$$

which corresponds to two total band counts observed at the upper redshift limit for the normal galaxies: $z = 0.6$. The most luminous detected sources at lower redshifts, with $10^{41} \text{ erg s}^{-1} < L_x < 10^{42} \text{ erg s}^{-1}$, are within the range possible for star forming galaxies, (e.g., Norman et al. 2004). Moreover, our bootstrap uncertainty estimates are close to the Poisson limits, which means that the X-ray flux cannot be dominated by a small number of luminous sources.

As an additional check on our ability to detect galaxies and to diagnose problems with background subtraction or contamination, we constructed a null sample to compare with the fluxes of the real sources. To create the null sample we kept the redshifts and (optical) luminosities of the galaxies fixed but assigned them random positions in the field, excluding locations closer than 60 kpc to an AGES galaxy. We then analyzed the random catalog in the same manner as the actual data. In Figure 3, we compare the luminosities of the real galaxies and the “empty” regions. While the real galaxies generate a significant signal in all but the faintest ($M_R \gtrsim -18$) bins, the mean luminosities of the random fields are always consistent with zero. The uncertainties in the random signal closely follow the expected trend of $\Phi_{\min} 4\pi d_L^2(z)$, where $\Phi_{\min} \approx 4 \times 10^{-17} \text{ erg s}^{-1} \text{ cm}^{-2}$ is the sensitivity of the observations divided by the square root of the number of galaxies in a typical bin. Stacking the galaxies in our luminosity and redshift bins generally provides $\gtrsim 25$ times the sensitivity associated with the 5 ks exposure time for individual sources. Over the range of redshifts we probe, this flux limit corresponds to threshold luminosities of $\approx 10^{38} \text{ erg s}^{-1}$ to $10^{40} \text{ erg s}^{-1}$.

The X-ray properties of our stacked galaxy samples are summarized in Tables 2 and 3. Table 2 provides upper limits on the hard and soft band X-ray luminosities of the optically faintest AGES galaxies that were either not detected in X-rays or had net stacked emission with $S/N < 1$ in all X-ray bands. Table 3 provides the data for the detected ($S/N > 1$) galaxies.

3.1. Monte Carlo Simulations

We used Monte Carlo simulations to test our analysis methods and to refine our choices of parameters. We started by generating a mock galaxy catalog using the Brown et al. (2001) R -band luminosity function, a simple model for galaxy evolution, and the AGES main galaxy sample selection criteria including the sparse sampling. The general properties of the resulting synthetic catalog are quite similar to those of the real one. The absolute magnitude strips are a case in point. From faint to bright magnitudes, the real strips with integral, absolute magnitude boundaries in Figure 1 contain 471, 1621, 2526 and 1496 galaxies including the corrections for sparse sampling,

while the corresponding strips in the synthetic catalog contain 614, 1630, 2218 and 1527 galaxies.

To simulate the X-ray data, we began by distributing $\approx 350,000$ background photons at random positions in the field with surface densities of 1.9×10^{-3} hard (2–7 keV) and 0.9×10^{-3} soft (0.5–2 keV) photons arcsec $^{-2}$, based on the background estimates for the XBoötes survey (Kenter et al. 2005). We then assigned each galaxy an extended X-ray component and a point-like nucleus. For simplicity, the extended emission consists solely of soft photons and the AGN component consists solely of hard photons. These components have mean luminosities of

$$\begin{aligned} L_{x40,\text{soft}} &= 5(L/L_*)(1+z)^3 \\ L_{x40,\text{hard}} &= 5(L/L_*)(1+z)^4, \end{aligned} \quad (9)$$

respectively, in units of 10^{40} erg s $^{-1}$, where L/L_* is the rest-frame (*R*-band) optical luminosity in units of the characteristic luminosity, L_* , at the knee of the Schechter luminosity function. The redshift scaling and the correlation between the X-ray and optical luminosities are motivated both by previous studies (e.g., David, Jones, & Forman 1992; Shapley et al. 2001, Brand et al. 2005) and by our own results (see Section 4).

Based on the X-ray spectrum of the AGES galaxies, we converted the X-ray fluxes to counts using soft and hard band flux limits of 1.05×10^{-15} erg cm $^{-2}$ s $^{-1}$ and 3.65×10^{-15} erg cm $^{-2}$ s $^{-1}$, respectively and K-corrections of $(1+z)^{\Gamma-2}$, with $\Gamma = 1.29$ (see Section 2.1). The hard emission was distributed about the galactic centers using a Gaussian model of the *Chandra X-ray Observatory* PSF with a 50% enclosed energy radius of

$$r_{\text{PSF}} = 0''.5 + 6''.0 \left(\frac{D}{10'} \right)^2, \quad (10)$$

where D is the randomly assigned distance of the galaxy from the *Chandra X-ray Observatory* pointing center in arcminutes (see the *Chandra X-ray Observatory* Proposers' Guide¹⁰). We modeled the extended emission as a Gaussian of dispersion $r_L = 10(L/L_*)^{1/2}$ kpc convolved with the PSF to get an overall radial profile of

$$P_{\text{extended}}(R) \propto \exp \left[\frac{-R^2}{2(r_L^2 + r_{\text{PSF}}^2)} \right]. \quad (11)$$

In this model the X-ray surface brightness of the galaxies is independent of optical luminosity.

3.2. Radial Emission Profiles

We first verified that our analysis correctly extracts the X-ray emission profiles by analyzing the data for the roughly 800 galaxies in the mock catalog with $z \leq 0.1$ (mean redshift $\langle z \rangle \simeq 0.07$) and within $10'$ of the pointing center. We consider only these lower redshift sources because, in spite of the *Chandra X-ray Observatory's* high, on-axis resolution, the field-averaged PSF still approaches 2 kpc at $z \simeq 0.07$. Figure 4 shows the extracted profile for the total band. Using a 30 kpc signal aperture and a 30–60 kpc background subtraction annulus, we recover the input profile (and background level) to within the 1σ bootstrap uncertainties. We carry out a similar analysis on the real data in Section 4.1.

¹⁰ <http://cxc.harvard.edu/proposer/POG/html>

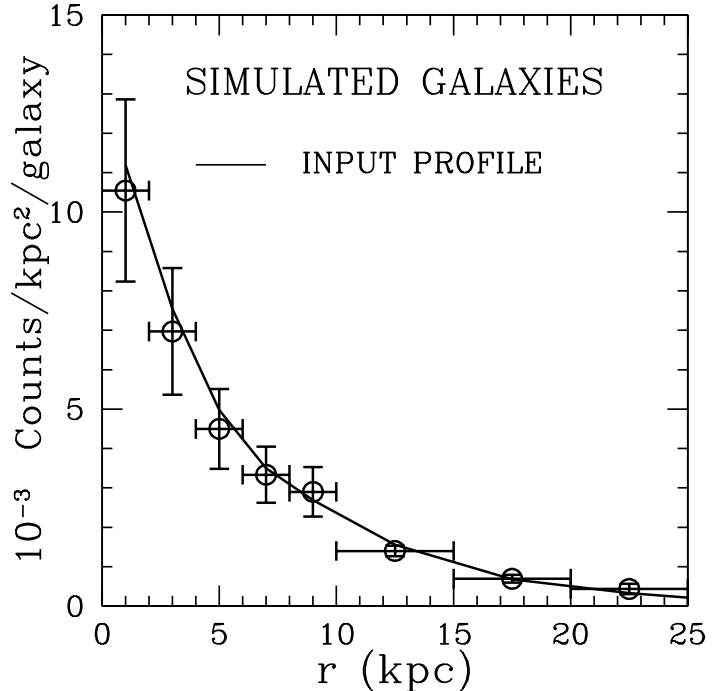


FIG. 4.— Monte Carlo test of the stacking procedure. The solid curve shows the input total band emission profile in our Monte Carlo simulation, and the open circles show the profile extracted by the stacking analysis. The extracted profile agrees with the input profile in all radial bins.

At higher redshifts, where we cannot spatially resolve the emission, we concentrate on extracting the redshift evolution of the X-ray luminosity. This involves a trade-off between the signal-to-noise ratio (S/N) and the need for aperture corrections. Larger apertures capture more signal but introduce extra noise from the background, while small apertures lose some of the signal and require more substantial aperture corrections. Redshift-dependent biases will be minimized by using a fixed angular aperture for point sources and a (sufficiently large) fixed physical aperture for extended sources. Since we expect a significant contribution from extended emission in the real data (e.g., Figure 2), we focused on fixed physical apertures with proper radii of $R_{\text{ap}} = 10, 20, 30, 40,$ and 50 kpc and background annuli extending over the larger of 30–60 kpc or $R_{\text{ap}}-2R_{\text{ap}}$. Adopting a signal aperture of $R_{\text{ap}} = 30$ kpc (at the mean redshift of each bin) led to the most accurate reproduction of the input profiles with the highest S/N; our detection criterion is $S/N > 1$. This fixed physical aperture corresponds to angular apertures of $\sim 15''-5''$ over the range of mean redshifts we analyze ($0.1 < z < 0.5$, see Table 2 and Figure 2). The size of the field-averaged PSF begins to exceed that of significantly smaller apertures, particularly in the higher redshift bins (see Figure 2). For point sources we could apply a redshift-dependent aperture correction to remedy this problem, but it is impossible to do so for extended sources when we are uncertain of their intrinsic profiles. For larger apertures, our signal-to-noise ratio begins to drop due to the increasing fraction of background photons included in the signal region. In the Monte Carlo simulations, small deviations ($\lesssim 10$ kpc) from $R_{\text{ap}} = 30$ kpc have little effect on the results or the signal-to-noise

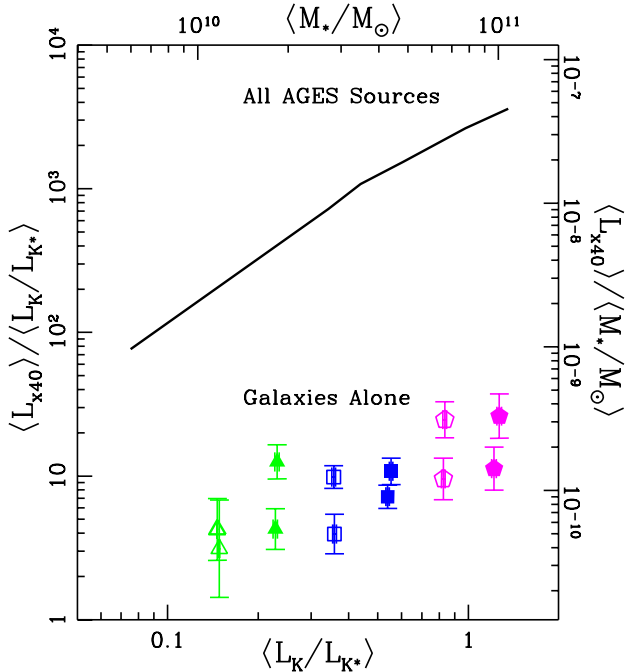


FIG. 5.— Specific X-ray luminosity of all AGES sources compared to that of the normal galaxy sample. The solid line is a fit to the sum of the mean luminosity of the normal galaxies and the mean luminosity of the 58 X-ray detected AGNs (see Section 2.2 and Tables 1 and 3) that lie within the absolute magnitude and redshift ranges we consider. The binned data shows the mean luminosity evolution of the normal galaxies alone; the point type conventions are the same as those used in Figure 3. The two points at each value of L_K demonstrate the evolution from the low to high redshift bin in each absolute magnitude strip (Figure 1).

ratio but larger (factor of 2) changes in the aperture lead to serious problems.

Using $R_{\text{ap}} = 30$ kpc and 30–60 kpc background annuli, which we adopt throughout the remainder of the paper, we successfully recover the input luminosity evolution (Eqn. 9); i.e., when we fit our results with a double power law model (Eqn. 5), we find scalings for the soft and hard band X-ray luminosities that are statistically consistent with the input evolution rates and normalization:

$$L_{x40,\text{soft}} = (4.7 \pm 1.7) \left(\frac{L_K}{L_{K^*}} \right)^{1.0 \pm 0.2} (1+z)^{2.7 \pm 0.8},$$

$$L_{x40,\text{hard}} = (4.0 \pm 2.4) \left(\frac{L_K}{L_{K^*}} \right)^{0.9 \pm 0.3} (1+z)^{3.4 \pm 1.1}. \quad (12)$$

4. RESULTS

We now turn to the real sources, starting with a comparison of the X-ray emission from normal galaxies and from spectroscopic AGNs. Figure 5 shows the specific X-ray luminosity, $\langle L_{x40} \rangle / \langle L_K/L_{K^*} \rangle$, as a function of $\langle L_K/L_{K^*} \rangle$ for both the normal galaxies and the full sample including the X-ray and spectroscopically flagged AGNs. With the top and right axes, we also show the inferred scaling with stellar mass, based on Eqn. (3), although this conversion does not apply when the bright AGNs dominate the K -band flux. While the AGNs have significantly larger X-ray luminosities than the “normal” galaxies, the “normal”

galaxies are clearly detected. The two points at each L_K show the evolution of the normal galaxy X-ray emission from the low to high redshift bin in each absolute magnitude strip (Figure 1). When we fit the normal galaxy data as a double power law in K -band luminosity and redshift (Eqn. 5), we find that

$$L_{x40} = (6.0 \pm 1.0) \left(\frac{L_K}{L_{K^*}} \right)^{1.1 \pm 0.2} (1+z)^{3.2 \pm 0.8},$$

$$L_{x40,\text{hard}} = (4.6 \pm 0.9) \left(\frac{L_K}{L_{K^*}} \right)^{1.2 \pm 0.3} (1+z)^{3.5 \pm 1.0},$$

$$L_{x40,\text{soft}} = (2.0 \pm 0.5) \left(\frac{L_K}{L_{K^*}} \right)^{1.1 \pm 0.2} (1+z)^{2.7 \pm 0.7} \quad (13)$$

for the total, hard, and soft X-ray bands, respectively, in units of 10^{40} erg s^{-1} . Because our results indicate that L_x is roughly proportional to L_K in all X-ray bands, the specific X-ray luminosities of the galaxies should evolve similarly regardless of their optical luminosity or mass.

The X-ray luminosities we measure are roughly an order of magnitude brighter than the contribution expected from LMXBs (Eqn. 2), so we are left with three major candidates for the origin of the emission—HMXBs associated with recent star formation, accretion onto SMBHs (AGNs), and hot gas. We use three tests to try to determine the dominant source(s). We first use fits to the AGES spectra to divide the normal galaxies into late-type and early-type subsamples. Doing so allows us to compare the X-ray emission from galaxies with and without (optical) spectroscopic signatures of star formation. The resulting subsamples contain 3178 late-type galaxies and 2968 early-type galaxies. Second, we examine the radial emission profiles of the low redshift galaxies, since emission due to star formation and hot gas will be more spatially extended than emission from AGNs. Third, we compare the hardness ratios of the galaxies, in terms of the hard and soft band counts C_{hard} and C_{soft} , $\text{HR} = (C_{\text{hard}} - C_{\text{soft}}) / (C_{\text{hard}} + C_{\text{soft}})$, to the typical values expected for X-ray binaries, AGNs, and hot gas.

4.1. Radial Emission Profiles

Figure 6 shows the average, background-subtracted soft, hard, and total band emission profiles of 488 (360 late-type and 128 early-type) low redshift ($z < 0.1$), galaxies within $10'$ of the *Chandra X-ray Observatory* optical axis, excluding X-ray sources that violate our luminosity limit (Eqn. 8) and AGNs identified through optical spectroscopy. The mean redshift of these galaxies is $\langle z \rangle \simeq 0.07$. Rather than use a model for the PSF (Eqn. 10), we determined it empirically by averaging the emission profiles of ≈ 500 $z > 1$ X-ray selected AGNs from the XBoötes survey. As with the galaxies, we used only AGN sources within $10'$ of the *Chandra* field centers and stacked the emission based on the optical positions. We then applied the angular corrections needed to put the PSF model on the same physical scale as the galaxies.

We find that the emission profiles of the late-type galaxies are clearly extended while those of the early-type galaxies have a more pronounced nuclear component. We use the Kolmogorov–Smirnov (K–S) test to compare the radial distribution of (total band) photons from the late-type galaxies, early-type galaxies, and high redshift AGNs.

Within 5 kpc of the stacking centers, we find that the early-type galaxy distribution ($\propto r^{-1.1}$) is consistent with the AGN distribution (K–S likelihood 97%), while the late-type galaxy distribution ($\propto r^{-0.4}$) is not (K–S likelihood 3%). However, if we analyze the full extraction region, neither galaxy profile is consistent with the AGN model (K–S likelihood $< 1\%$). Between 10 and 30 kpc, both galaxy types show significant ($\gtrsim 2.5 \sigma$) emission, which we attribute primarily to diffuse gas and LMXBs. Soft X-ray emitting gas has been observed out to $\gtrsim 20$ kpc around late-type (e.g., Strickland et al. 2004) and early-type (e.g., Mathews & Brighenti 2003) galaxies, as have LMXBs (late-type: e.g., Wang et al. 1999; early-type: e.g., Kim et al. 2006), leading to extended profiles like those in Figure 6. Our results imply that the emission from the low-redshift early-type galaxies comes from a combination of AGNs, hot gas, and LMXBs. In contrast, because the emission from the late-type galaxies is significantly less centrally concentrated than the emission of AGNs – even within a radius of 5 kpc – the dominant source of the late-type galaxy flux is most likely a radially extended distribution of HMXBs and LMXBs.

4.2. Hardness Ratios

In Figure 7, we show the HRs based on the hard- and soft-band counts of the two galaxy classes. To improve the statistical significance of our HRs, we combine hard and soft counts from bins of comparable redshifts in adjacent absolute magnitude strips (Figure 1). For reference, we compare these HRs to those observed in these bands for accreting binaries (HR $\gtrsim 0$, e.g., Munro et al. 2004), Type I AGNs (HR $\simeq -0.5$, e.g., Rosati et al. 2002; Franceschini, et al. 2005), Type II AGNs ($0 \leq \text{HR} \leq 1$, e.g., Rosati et al. 2002), and hot gas with a temperature of 0.5–1 keV (HR $\simeq -1$).

In general, we observe that the late-type galaxies have slightly harder spectra than the early-type galaxies and that the spectra of both galaxy types become somewhat harder with increasing redshift. This is most likely a consequence of the larger amount of soft X-ray emitting gas in earlier type galaxies and the steadily increasing contributions of HMXBs and AGNs, respectively, to the late-type and early-type galaxy spectra at higher redshifts.

4.3. Luminosity Evolution

To isolate the dependence of L_x on L_K , we examined the evolution of the X-ray luminosity of the early and late-type galaxies in three narrow redshift slices: $\langle z \rangle = 0.20 \pm 0.02$, $\langle z \rangle = 0.25 \pm 0.02$, and $\langle z \rangle = 0.35 \pm 0.03$. As shown in Figure 8, the specific X-ray luminosities are relatively flat in L_K , indicating an approximately linear correlation between L_x and L_K as found previously (e.g., David, Jones, & Forman 1992; Shapley et al. 2001). If we fit these results with a power law model, $L_x \propto L_K^\alpha$, we find consistent values of α among the three redshift slices for both the late-type ($\alpha_{\text{hard}}^{\text{LATE}} = 1.19 \pm 0.31$; $\alpha_{\text{soft}}^{\text{LATE}} = 1.12 \pm 0.15$) and early-type ($\alpha_{\text{hard}}^{\text{EARLY}} = 1.09 \pm 0.23$; $\alpha_{\text{soft}}^{\text{EARLY}} = 1.07 \pm 0.15$) galaxies.

Figures 9 and 10 illustrate the dependence of the specific X-ray luminosity of the late-type and early-type galaxies, respectively, on redshift (left panels) and optical luminosity (right panels). If we fit the late-type galaxies with the

double power-law model (Eqn. 5), we find that, in units of $10^{40} \text{ erg s}^{-1}$,

$$L_{x40,\text{hard}}^{\text{LATE}} = (5.9 \pm 1.6) \left(\frac{L_K}{L_{K*}} \right)^{1.2 \pm 0.4} (1+z)^{3.6 \pm 1.2},$$

$$L_{x40,\text{soft}}^{\text{LATE}} = (2.5 \pm 0.6) \left(\frac{L_K}{L_{K*}} \right)^{1.1 \pm 0.2} (1+z)^{2.2 \pm 1.0} \quad (14)$$

The reduced χ^2 (per degree of freedom) for these fits are 0.78 and 0.81 for the hard and soft bands, respectively. If we fit the early-type galaxies, we find that

$$L_{x40,\text{hard}}^{\text{EARLY}} = (3.0 \pm 0.6) \left(\frac{L_K}{L_{K*}} \right)^{1.0 \pm 0.3} (1+z)^{3.9 \pm 0.8},$$

$$L_{x40,\text{soft}}^{\text{EARLY}} = (1.8 \pm 0.4) \left(\frac{L_K}{L_{K*}} \right)^{1.1 \pm 0.2} (1+z)^{3.1 \pm 0.8} \quad (15)$$

In this case, the reduced χ^2 values are 0.86 and 1.14 for the hard and soft bands, respectively. The reduced χ^2 values for the best-fit curves given in the remainder of the paper are all similarly good, i.e., $\approx 1 \pm 0.2$. In all cases, the upper limits set by non-detections (bins with S/N < 1) are used in conjunction with detections to establish the best-fit curves. In particular, if any best-fit curves exceed these upper limits, the squared difference is added to the χ^2 sum.

The results for the individual luminosity and redshift bins are summarized in Tables 2 and 3. In spite of the evidence that different physical processes dominate the emission of the late-type and early-type galaxies, the two populations exhibit qualitatively similar behaviors. In particular,

- the X-ray luminosity monotonically increases from low mass galaxies at low redshift to high mass galaxies at high redshift and
- the X-ray luminosity is significantly higher than what would be expected from LMXBs on the basis of the K -band luminosities, Eqn. (2), assuming a hardness ratio of HR = 0 (e.g., Munro et al. 2004).

These similarities are not surprising, as we expect the X-ray emission of LMXBs and hot gas to be nearly time-independent for $z \lesssim 0.5$, while the HMXB and AGN emission should be evolving rapidly and at approximately the same rate ($\propto (1+z)^{3 \pm 1}$, e.g., David, Jones, & Forman 1992; Shapley et al. 2001, Hogg 2001, Norman et al. 2004, and Schiminovich et al. 2005 and Ba01 and Ba05, respectively).

4.4. Comparisons to Previous Work

In general, we find excellent agreement between our results and those of earlier studies of normal galaxy X-ray evolution, but our uncertainties are smaller. There are three general categories of earlier results: surveys of nearby, individual galaxies, stacking analyses of low to intermediate-redshift galaxies and stacking analyses of intermediate to high-redshift galaxies in small-area, deep fields (CDF-N and CDF-S). Taking the late-type and early-type galaxies in turn, we first consider the Shapley et al. (2001, S01) and O’Sullivan et al. (2001, OS01) surveys of local spiral and early-type galaxies. Second, we compare our results to the Georgakakis et al. (2003, G03) stacking analysis of 2dF galaxies at $z \simeq 0.1$ and to our own earlier stacking analysis of massive early-type galaxies at $0.3 \lesssim$

$z \lesssim 0.9$ (B05). Finally, we consider the Hornschemeier et al. (2002, H02) and Lehmer et al. (2007) stacking analyses of normal galaxies in the CDF-N at $0.4 \lesssim z \lesssim 1.5$ and optically bright early-type galaxies in the extended CDF-S out to $z \lesssim 0.7$, respectively.

Shapley et al. (2001, S01) studied the correlation between the X-ray (0.2–4.0 keV) and H -band flux of 234 local spiral galaxies with no sign of AGN activity. Their results indicate a trend of

$$L_{x40,S01}^{\text{LATE}}(z \simeq 0) \simeq (2 \pm 1) \left(\frac{L_K}{L_{K*}} \right)^{1.2 \pm 0.1}, \quad (16)$$

assuming $H-K = 0.27$ mag and a 50% uncertainty in the normalization of the correlation. It is clear that Eqn. (16) agrees very well with Eqn (14) at $z = 0$, and, as shown in Figure 9, the agreement extends to all redshifts if we allow for evolution (see Figure 9). Similar trends have been found in other local surveys (e.g., David, Jones, & Forman 1992).

Georgakakis et al. (2003, G03) considered 200 galaxies in the 2dF redshift survey with $\langle L_B \rangle \simeq L_*$ at a mean redshift $\langle z \rangle \simeq 0.1$. They measured mean soft band luminosities of $\log(L_x/\text{erg s}^{-1}) \simeq 40.2 \pm 0.2$, 39.7 ± 0.4 and 40.5 ± 0.2 for the combined, late-type and early-type samples. They also estimated an upper limit of $\log(L_x/\text{erg s}^{-1}) \lesssim 40.5$ on the hard band luminosities of the samples. These results are consistent with ours, particularly if we allow for positive redshift evolution of the X-ray luminosity between $\langle z \rangle \simeq 0.1$ for G03 and our points for galaxies of similar optical luminosities at $z \simeq 0.25$ and 0.45 .

Hornschemeier et al. (2002, H02) conducted a stacking analysis of late-type galaxies in the HDF-N/CDF-N, finding that 29, $\simeq 0.7L_*$ galaxies in the redshift range $0.4 - 0.75$ have mean total (0.5 – 8 keV) and soft band (0.5–2.0 keV) luminosities of $L_{x40} = 2.9 \pm 0.4$ and 1.3 ± 0.2 , respectively. These too are consistent with the values we find for $\simeq 0.7L_*$ galaxies at $0.2 \lesssim z \lesssim 0.3$ (3.6 ± 0.8 and 1.6 ± 0.3 , respectively).

Turning to the early-type galaxies, we first checked the relative contributions of hot gas and AGN emission by comparing our results to the ROSAT PSPC (0.1–2.5 keV) X-ray survey of 401 local early-type galaxies discussed in O’Sullivan et al. (2001). Because the hot gas emission from the early-type galaxies is primarily a function of galaxy mass rather than epoch, there should be little difference between the soft band flux of the local and AGES galaxies (at $0.15 \lesssim \langle z \rangle \lesssim 0.45$), provided that the soft band AGN contamination in the AGES sample is small. Figure 10 shows that the soft band luminosity from the AGES early-type galaxies is, in fact, comparable to that of the local sample even at high optical luminosities (which tend to be associated with higher redshifts in the AGES sample). In contrast, the total luminosity of the AGES early-type galaxies is consistently higher than that of the local sample. Figure 10 also demonstrates that the hard X-ray component of the early-type galaxies is well in excess of the estimated LMXB emission and undergoes rapid, positive redshift evolution. These findings reinforce our conclusions in Section 4.2, that the soft band flux of the AGES early-type galaxies comes primarily from hot gas, while the more rapidly evolving hard component comes primarily from AGNs.

Our results for the massive ($\sim L_*$) early-type galaxies

agree with those of G03 and with our earlier work (B05), where we found that bright red ($M_R < -21.3$) galaxies at $z \simeq 0.4$ had total X-ray luminosities of $L_x \simeq 10^{41} \text{erg s}^{-1}$. By incorporating the results of G03 and B05 with ours, we gain more leverage on the behavior of L_* early-type galaxies at lower ($z \simeq 0.1$) and higher ($0.5 \lesssim z \lesssim 0.9$) redshifts than what we can probe with AGES alone. Using this combined sample, we find that the hard and soft band luminosities of L_* early-type galaxies follow the trends

$$L_{x40,\text{hard}}^{\text{EARLY}}(L_*) = (3.6 \pm 1.5)(1+z)^{4.5 \pm 1.7} \quad (17)$$

and

$$L_{x40,\text{soft}}^{\text{EARLY}}(L_*) = (2.0 \pm 0.8)(1+z)^{2.8 \pm 1.1} \quad (18)$$

out to $z \simeq 1$. These global fits, which are shown in Figure 11, are consistent with those found for the AGES L_* early-type galaxies alone (Eqn. 15 at $L_K = L_{K*}$).

Lehmer et al. (2007) conducted a stacking analysis of 222 optically bright ($\sim L_{B*}$) early-type galaxies in the E-CDF-S with photometric redshifts ranging from 0 to 0.7. The mean hard X-ray luminosity trend inferred for AGNs in the Lehmer et al. galaxy sample is in excellent agreement with the hard band trend found in B05 (see Lehmer et al. 2007; Figure 13) and in the present paper (Figure 11).

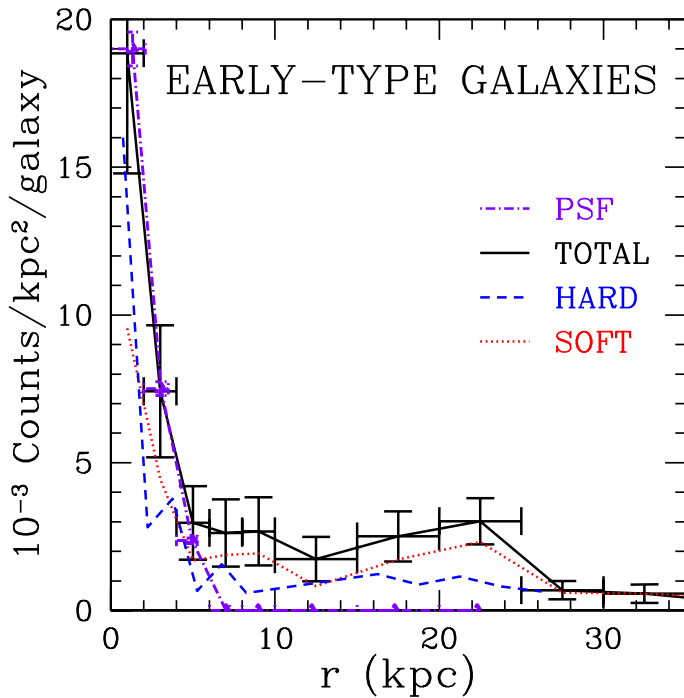
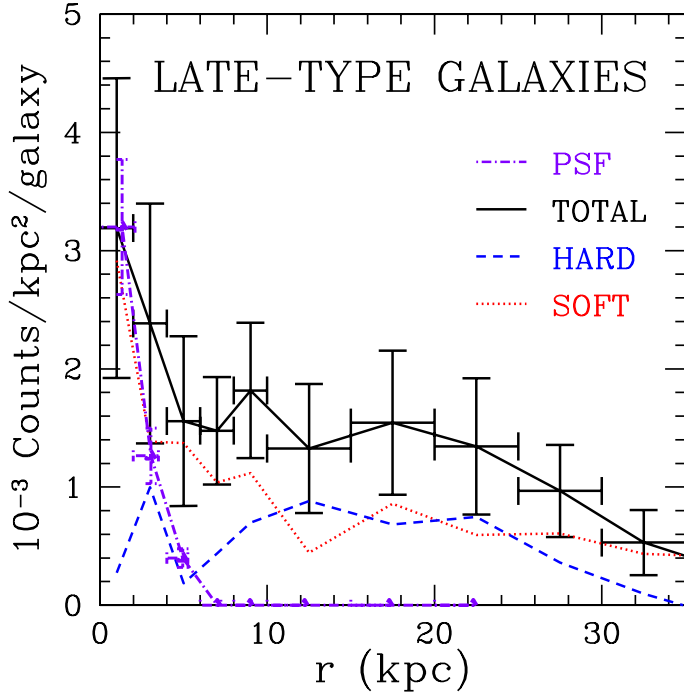


FIG. 6.— Background-subtracted radial emission profiles of 360 late-type (top) and 128 early-type (bottom) galaxies with $z \leq 0.1$, a mean redshift of $\langle z \rangle \approx 0.07$ and within $10'$ of *Chandra X-ray Observatory* field centers. The solid, dashed, and dotted curves represent the total, hard, and soft band profiles, respectively, in each panel. The dot-dashed curve shows an empirical model of the PSF, based on the radial emission of ≈ 500 , $z \gtrsim 1$ AGNs within $10'$ of a *Chandra X-ray Observatory* field center. We have shifted the normalization of the PSF model to match the amplitude of the galaxy profile in each panel.

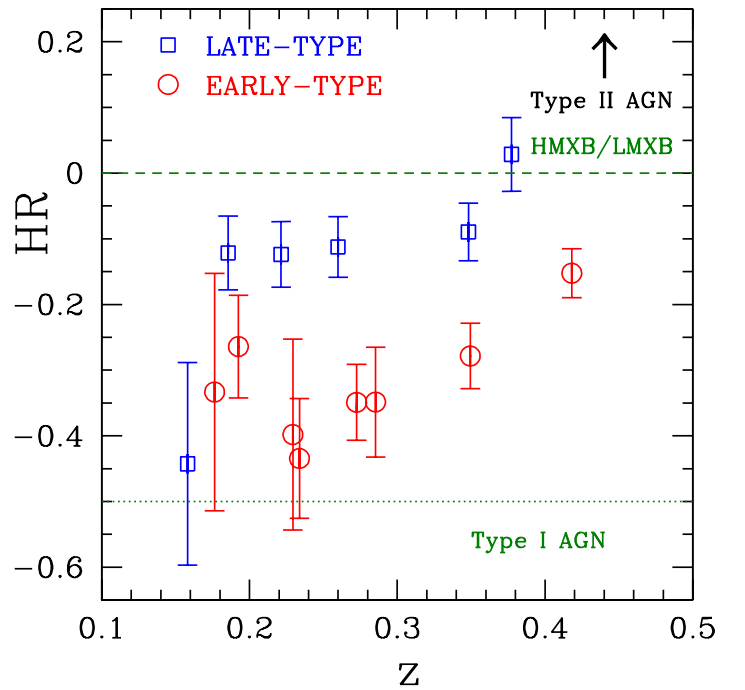


FIG. 7.— Redshift evolution of the hardness ratio (HR) for the late-type (squares) and early-type (circles) samples of galaxies. The late-type galaxies exhibit slightly harder spectra than the early-type galaxies, which is most likely due to the early-types' characteristically larger halos of soft X-ray emitting gas. Typical HRs of HMXBs and LMXBs (dashed line) as well as Type I (dotted line) and Type II AGNs (typically above the dashed line) have been included for reference.

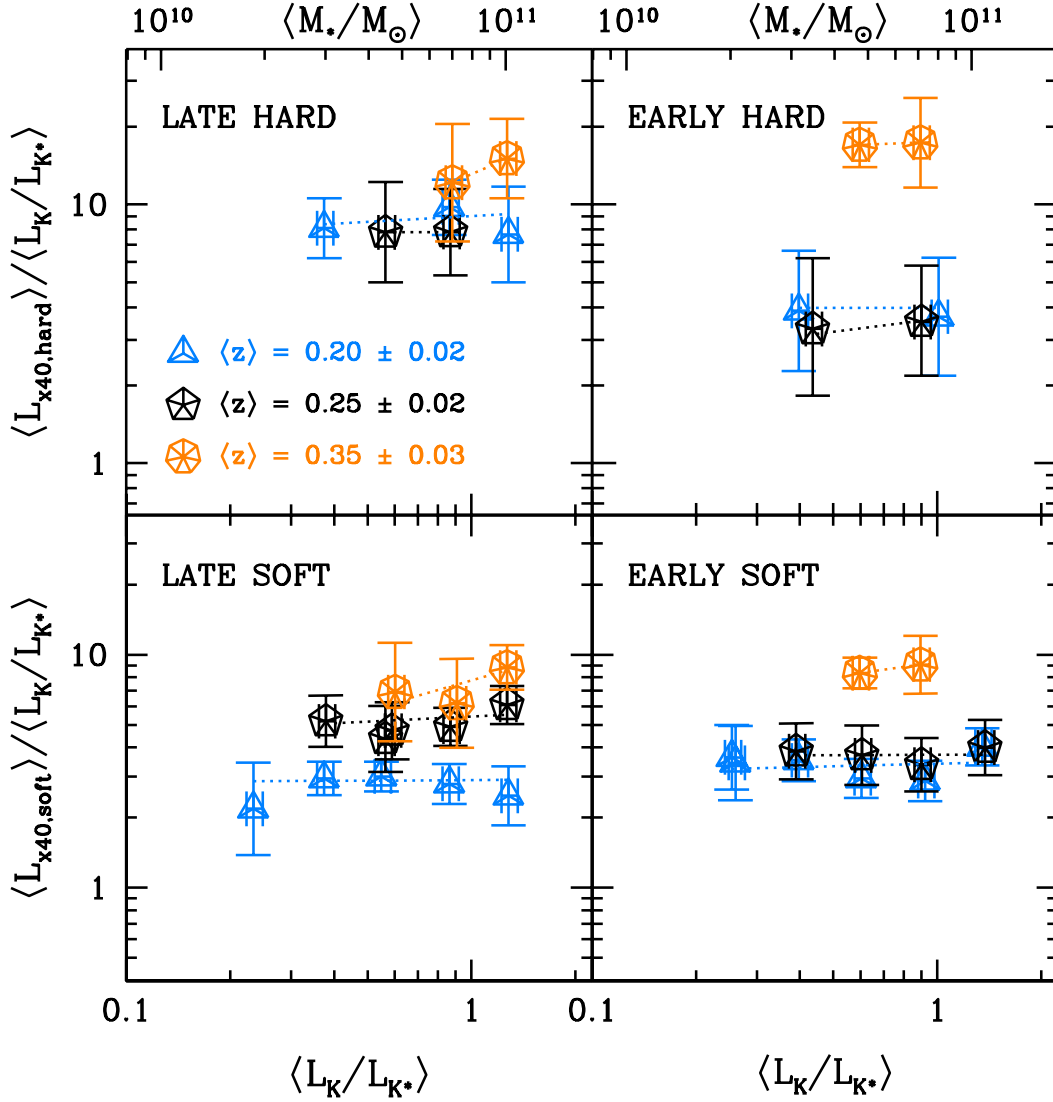


FIG. 8.— Specific X-ray luminosity evolution of the early and late-type galaxies in three narrow redshift slices: $\langle z \rangle = 0.20 \pm 0.02$ (three-pointed stars), $\langle z \rangle = 0.25 \pm 0.02$ (five-pointed stars), and $\langle z \rangle = 0.35 \pm 0.03$ (seven-pointed stars). In all redshift slices, the specific X-ray luminosities are relatively flat in L_K (roughly, $L_{x,late} \propto L_K^{1.2 \pm 0.3} \propto L_{x,early}$, see Section 4.3), indicating an approximately linear correlation between L_x and L_K as found previously (e.g., David, Jones, & Forman 1992, Shapley et al. 2001).

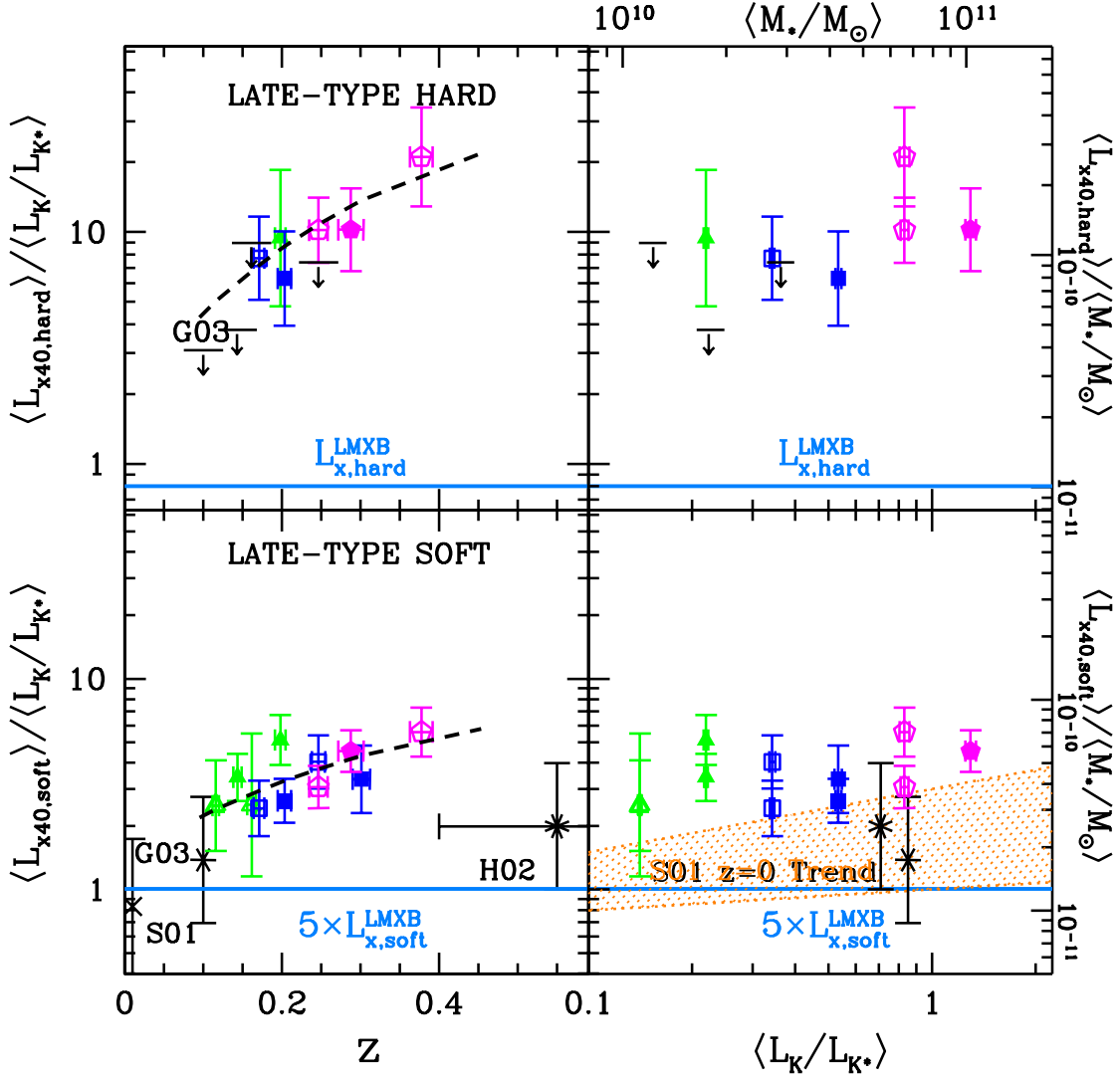


FIG. 9.— **Left:** the mean hard and soft band specific X-ray luminosities of the late-type sample of galaxies as a function of redshift. The point type conventions are the same as those used in Figure 3. The best-fit curves for the hard and soft band emission are also shown. **Right:** the mean hard and soft specific X-ray luminosities as a function of $\langle L_K \rangle$ for the late-type sample of galaxies. The instances in which there are two points at each value of L_K demonstrate the evolution from the low to the high redshift bin in the corresponding absolute magnitude strip (Figure 1). Top and right axes display the corresponding behavior of $\langle L_x \rangle / \langle M_* \rangle$ vs. $\langle M_* \rangle$ based on Eqn. 3. Upper limits (1σ) are provided in the hard band panels for bins with negative net counts (see Table 2). For comparison, we have plotted the specific X-ray luminosities found by Shapley et al. (2001, S01, four-pointed star at $z \approx 0$), Georgakakis et al. (2003, G03, six-pointed star in the soft-band panel; upper limit in the hard-band panel at $z \approx 0.1$), and Hornschemeier et al. (2002, H02, 8-pointed star at $z \approx 0.55 \pm 0.15$). The shaded region in the lower right panel shows the local S01 $L_{x,soft}(L_K)$ trend, roughly $\log(L_{x40}) = (0.3 \pm 0.2) + (1.2 \pm 0.1) \log(L_K/L_{K^*})$, which encompasses both the scatter in and error bars on the S01 data points.

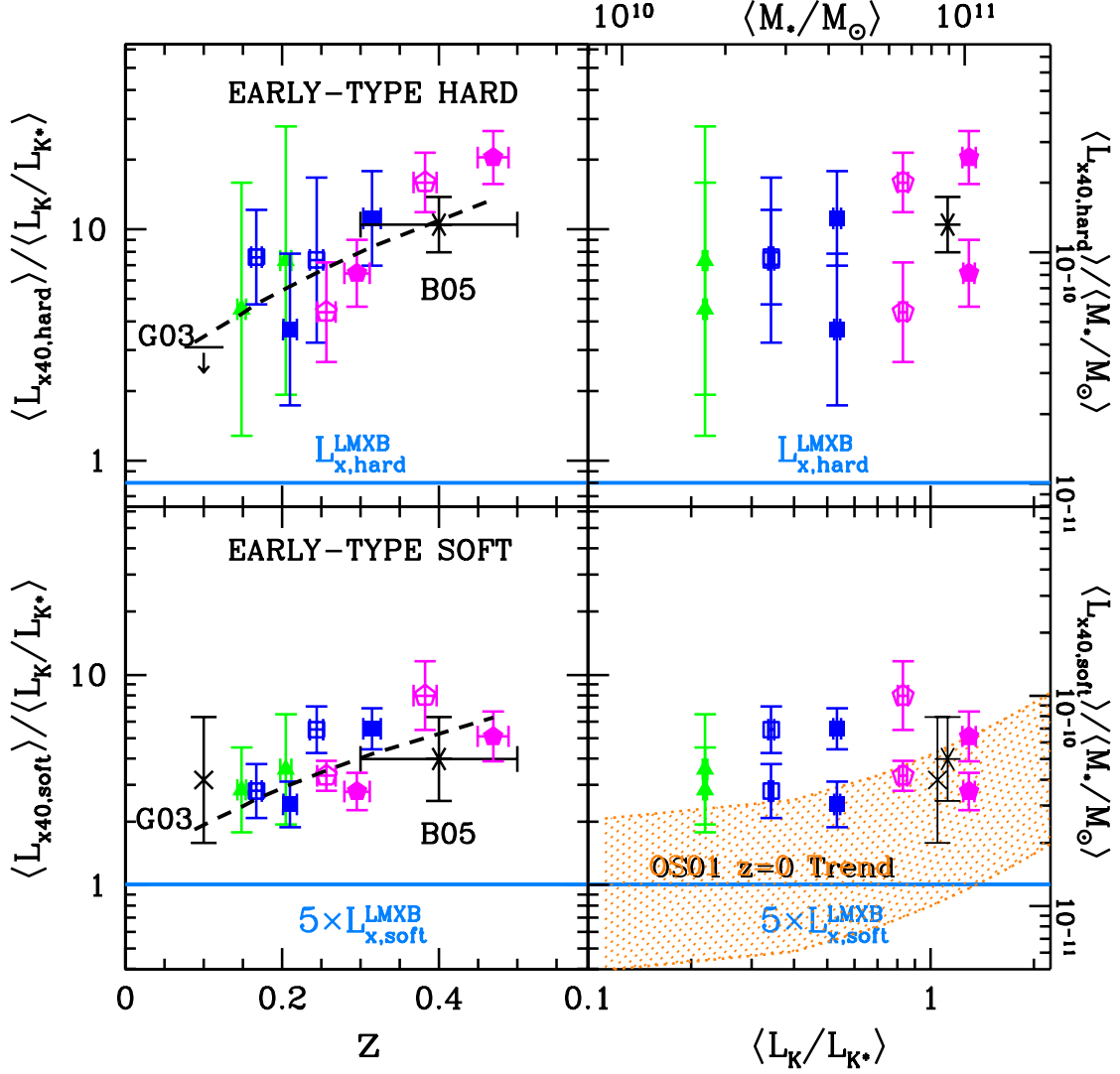


FIG. 10.— Same as Figure 9 for the early-type sample of galaxies. For comparison, we have plotted the specific X-ray luminosities of $z \simeq 0.1$ L_* galaxies found by Georgakakis et al. (2003, G03, four-pointed star in the soft-band panel; upper limit in the hard band panel) and Brand et al. (2005, B05, six-pointed star in both panels at $z = 0.4 \pm 0.1$). The best-fit curve for soft- and hard-band emission from the AGES galaxies is also shown. The shaded region in the lower right panel shows the local O’Sullivan et al. (2001, OS01) $L_{x,soft}(L_K)$ trend, roughly $\log(L_{x40}) = (0.3 \pm 0.3) + (1.7 \pm 0.2) \log(L_K/L_{K*})$, which encompasses both the scatter in and error bars on the OS01 data points.

TABLE 1
X-RAY COUNTS FROM STACKED NORMAL GALAXIES & EXCLUDED AGN

Class	Source	Number of Objects	Net Hard Counts	Net Soft counts
Normal Galaxies	Late-Type Galaxies	3178	240	327
	Early-Type Galaxies	2968	246	342
Spectroscopic AGN	Broad Line AGN	27	319	872
	Narrow Line AGN	78	496	404
X-ray Sources	Broad Line AGN	24	319	872
	Narrow Line AGN	34	468	367

TABLE 2
X-RAY LUMINOSITY UPPER LIMITS FOR THE OPTICALLY FAINTEST AGES GALAXIES

$M_{R,\max}$ (mag)	$M_{R,\min}$ (mag)	$\langle z \rangle$	N_{galaxies}	L_{x40} (h/s)	
Late-Type Galaxies					
-17.5	-18.5	0.0693	126	< 0.6/	< 0.2
-17.5	-18.5	0.0951	126	< 1.9/	< 1.0
-18.0	-19.0	0.0969	228	< 1.2/	< 0.7
-18.0	-19.0	0.1286	228	< 1.2/	< 0.4
Early-Type Galaxies					
-17.5	-18.5	0.0756	13	< 1.8/	< 0.4
-17.5	-18.5	0.0882	13	< 2.2/	< 0.9
-18.0	-19.0	0.1051	59	< 2.6/	< 0.6
-18.0	-19.0	0.1303	56	< 3.4/	< 0.9
-18.5	-19.5	0.1166	119	< 2.4/	< 0.4
-18.5	-19.5	0.1586	119	< 3.5/	< 1.5

Note. — The range of absolute R -band magnitudes of the galaxies in a bin is $M_{R,\max} > M_R > M_{R,\min}$ and the mean redshift is $\langle z \rangle$. N_{galaxies} is the effective number of galaxies in the bin, including the correction for sparse sampling. The 1σ upper limits on the hard (h; 2–7 keV) and soft (s; 0.5–2 keV) band X-ray luminosities, L_{x40} , of the optically faintest AGES galaxies are given in units of 10^{40} erg s^{-1} in the final column.

TABLE 3
SUMMARY OF RESULTS

$\langle M_R \rangle / \langle M_K \rangle$ (mag)	$\langle z \rangle$	N_{galaxies}	Net Counts (h/s/t)	S/N (h/s/t)	L_{x40} (h/s/t)	$\langle L_{x40} \rangle / \langle L_K / L_{K*} \rangle$ (h/s/t)
Late-Type Galaxies						
-18.98/-21.31	0.1159	375	17/ 34/ 51	0.8/2.0/1.8	0.7/ 0.4/ 1.1	4.3/ 2.5/ 6.8
-19.02/-21.33	0.1614	376	- 1/ 17/ 16	—/1.3/0.7	< 1.4/ 0.4/ 0.3	< 9.2/ 2.5/ 1.8
-19.42/-21.75	0.1434	580	- 4/ 71/ 67	—/3.9/2.3	< 0.8/ 0.7/ 0.6	< 3.9/ 3.4/ 2.8
-19.47/-21.80	0.1979	576	27/ 52/ 79	1.5/3.6/3.4	2.1/ 1.1/ 3.2	9.4/ 5.1/14.5
-19.93/-22.25	0.1709	667	55/ 61/116	2.4/3.3/4.0	2.6/ 0.8/ 3.5	7.7/ 2.4/10.1
-19.94/-22.26	0.2464	667	- 23/ 45/ 22	—/3.4/1.0	< 2.6/ 1.4/ < 3.0	< 7.5/ 4.0/ < 9.0
-20.36/-22.68	0.2032	555	39/ 59/ 98	2.1/4.2/4.2	3.4/ 1.4/ 4.8	6.3/ 2.6/ 8.9
-20.44/-22.75	0.3011	556	3/ 30/ 33	0.2/2.7/1.9	0.6/ 1.8/ 2.4	1.1/ 3.3/ 4.4
-20.85/-23.16	0.2465	403	46/ 50/ 96	3.1/4.3/5.1	8.5/ 2.5/11.0	10.2/ 3.1/13.2
-20.90/-23.20	0.3774	403	36/ 34/ 70	3.6/3.7/5.1	17.5/ 4.6/22.2	21.1/ 5.6/26.6
-21.27/-23.57	0.2878	195	25/ 39/ 64	2.4/4.4/4.7	13.2/ 5.9/19.1	10.2/ 4.5/14.8
Early-Type Galaxies						
-19.55/-21.88	0.1482	328	14/ 31/ 45	0.8/2.2/2.0	1.0/ 0.6/ 1.6	4.5/ 2.8/ 7.3
-19.51/-21.84	0.2047	327	11/ 19/ 30	0.7/1.7/1.6	1.6/ 0.8/ 2.4	7.3/ 3.6/10.9
-19.99/-22.31	0.1672	560	47/ 62/109	2.1/3.4/3.8	2.6/ 1.0/ 3.6	7.6/ 2.8/10.4
-20.00/-22.32	0.2438	561	20/ 53/ 73	1.2/3.9/3.4	2.5/ 1.9/ 4.4	7.4/ 5.5/12.8
-20.45/-22.77	0.2102	804	31/ 72/103	1.3/4.0/3.5	2.0/ 1.3/ 3.3	3.7/ 2.4/ 6.1
-20.45/-22.76	0.3146	796	37/ 65/102	2.1/4.5/4.5	6.0/ 3.0/ 8.9	11.2/ 5.5/16.7
-20.90/-23.21	0.2564	844	38/103/141	2.0/6.1/5.6	3.6/ 2.8/ 6.4	4.4/ 3.3/ 7.7
-20.90/-23.20	0.3823	844	55/ 98/153	3.4/6.7/7.0	13.3/ 6.6/19.9	15.9/ 8.0/23.9
-21.33/-23.63	0.2954	594	45/ 69/114	3.0/4.9/5.5	8.4/ 3.6/12.0	6.5/ 2.8/ 9.2
-21.38/-23.67	0.4691	593	48/ 42/ 90	3.8/3.7/5.3	26.5/ 6.6/33.1	20.4/ 5.1/25.5

Note. — The mean R -band and K -band absolute magnitudes of the galaxies in a bin are $\langle M_R \rangle$ and $\langle M_K \rangle$ and the mean redshift is $\langle z \rangle$. N_{galaxies} is the effective number of galaxies in the bin, including the correction for sparse sampling. The Net Counts column gives the number of photons observed above background in the hard (h; 2–7 keV), soft (s; 0.5–2 keV) and total (t; 0.5–7 keV) bands; the corresponding signal-to-noise ratio (S/N) of the measurements appears in the adjacent column. (Our detection criterion is $S/N > 1$). L_{x40} is the mean X-ray luminosity in the hard, soft and total bands in units of 10^{40} erg s^{-1} , and the final column is the specific X-ray luminosity, $\langle L_{x40,(\text{h,s,t})} \rangle / \langle L_K / L_{K*} \rangle$, for each band. In the cases of negative net counts, 1σ upper limits have been provided. Only bins that contain ≥ 100 galaxies and have net stacked emission with $S/N > 1$ in at least one X-ray band have been included in the table.

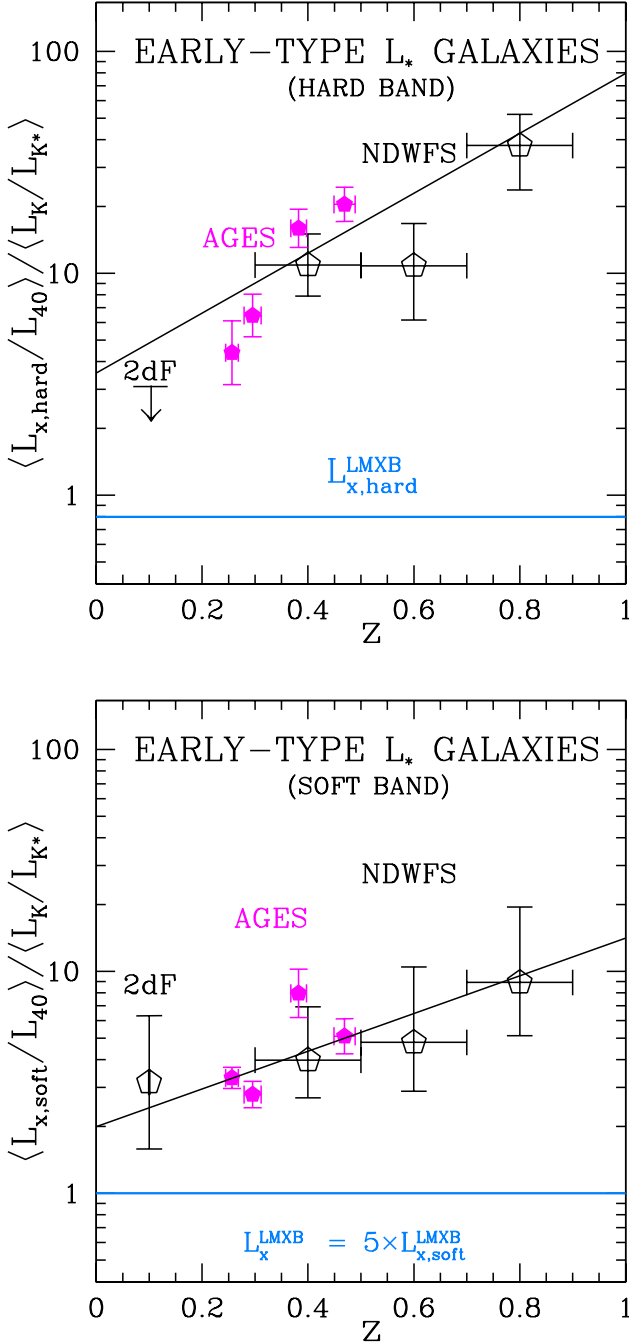


FIG. 11.— Mean hard (top) and soft (bottom) specific X-ray luminosities of $\simeq L_*$ early-type galaxies from G03 (2dF, $z = 0.1$), this work (AGES: filled points), and B05 (NDWFS: open points at $z \gtrsim 0.4$). The solid lines are global fits to the combined samples (see Section 4.4).

5. INTERPRETATION AS STAR FORMATION AND NUCLEAR ACCRETION

In this section, we interpret the trends in X-ray luminosity in terms of star formation (HMXBs) and nuclear accretion (AGNs) after estimating and subtracting the additional contributions of LMXBs and hot gas. Under the assumption, discussed in the introduction, that Eqn. 2 holds out to $z \simeq 0.5$, LMXBs represent a modest contribution to the emission from the late-type ($\lesssim 15\%$) and early-type

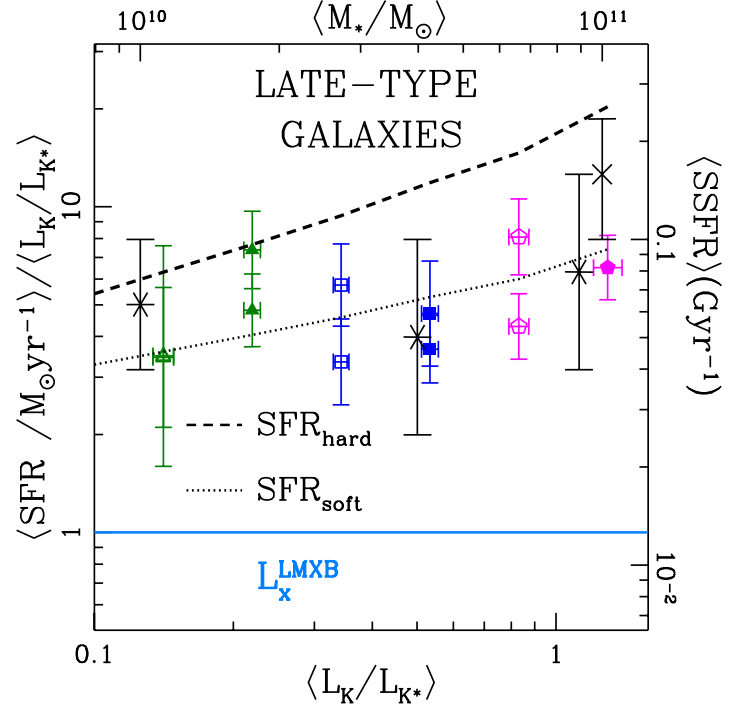


FIG. 12.— Specific star formation rate ($\text{SSFR} = \langle \text{SFR} \rangle / \langle M_* \rangle$) as a function of $\langle L_K \rangle$ and $\langle M_* \rangle$ based on the hard (dashed) and soft (dotted) X-ray luminosities of the AGES late-type galaxies and Eqns. (1) – (3). For the soft band values, the point-type conventions are the same as those used in Figure 3. We compare our results to those of Bauer et al. (2005) (six-pointed stars), and Bell et al. (2005) (four-pointed star).

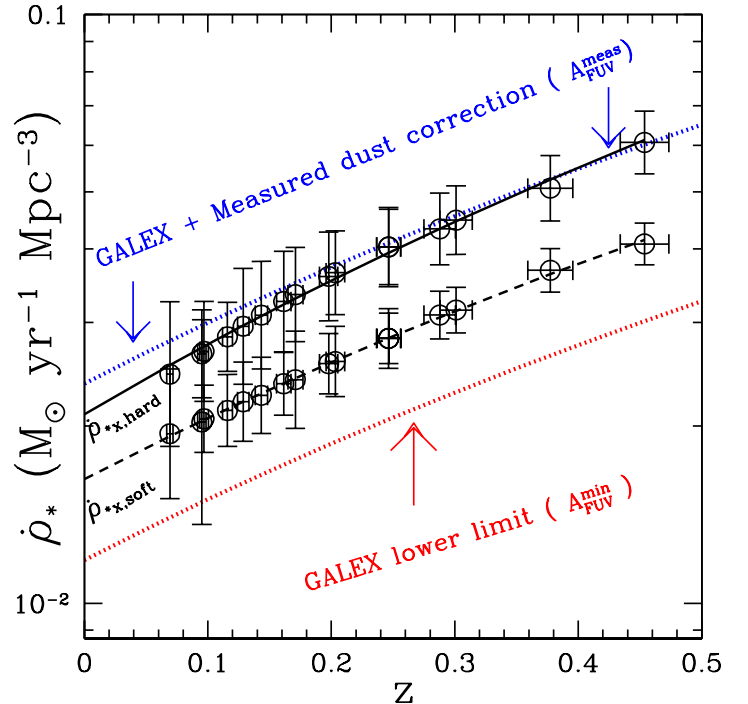


FIG. 13.— Estimates of the SFR density $\dot{\rho}_*$ based on the hard (solid) and soft (dashed) X-ray luminosities of the AGES late-type galaxies as compared to the GALEX results (Schiminovich et al. 2005) after either their minimum ($A_{\text{FUV}}^{\text{min}}$) or best-fit ($A_{\text{FUV}}^{\text{meas}}$) corrections for dust extinction have been applied.

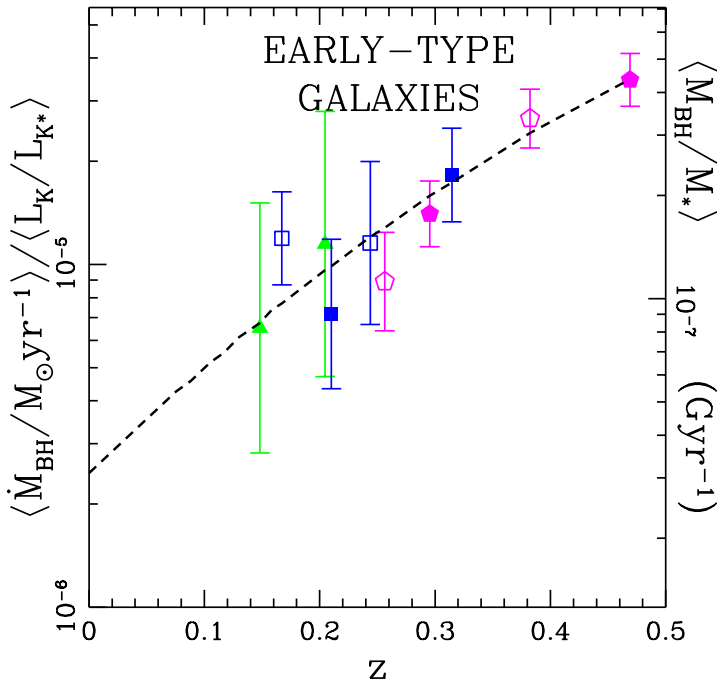


FIG. 14.— The specific SMBH accretion rate as a function of redshift based on the hard band X-ray luminosity of AGES early-type galaxies (in excess of LMXB emission) and Eqn. (4). The dashed line is the curve of best fit. The point type conventions are the same as those used in Figure 3.

($\approx 20\%$) galaxies. The comparison of the (primarily) hot gas emission from local early-type galaxies (O’Sullivan et al. 2001) shown in Figure 10 suggests that, at all redshifts, $\approx 50\%$ of the soft band (and $\lesssim 20\%$ of the total) emission of the AGES early-type galaxies is produced by hot gas. Based on these arguments, we conclude that $\gtrsim 85\%$ of the X-ray flux of the late-type galaxies is produced by HMXBs and $\gtrsim 60\%$ of the total (and $\gtrsim 80\%$ of the hard) X-ray flux of the early-type galaxies is produced by low luminosity AGNs. In the analysis that follows, we use the hard and soft band luminosities of the late-type galaxies to estimate the evolution of star formation rates in normal galaxies and the hard band luminosity of the early-type galaxies to estimate the growth rates of supermassive black holes in normal galaxies.

Before we can implement these assumptions, we must also consider the possibility that the flux from the high redshift late-type galaxies is being contaminated by AGNs. Since we cannot resolve their radial emission profiles as we did for the nearby subsamples (Section 4.1) and their luminosity evolution is fairly similar to that of the early-type galaxies, which we largely attribute to AGNs, we must find other ways to address this possibility. Fortunately, there are three key properties of the late-type galaxy emission that suggest the level of AGN contamination is small. First, the star formation signatures in the late-type galaxy optical spectra are necessarily correlated with a significant flux from HMXBs (Eqn. 1), suggesting that only a small fraction of the late-type galaxy emission could come from AGNs. Second, the X-ray emission from late-type galaxies is extended at low redshifts (Figure 6), directly demonstrating the absence of AGNs among the nearby members

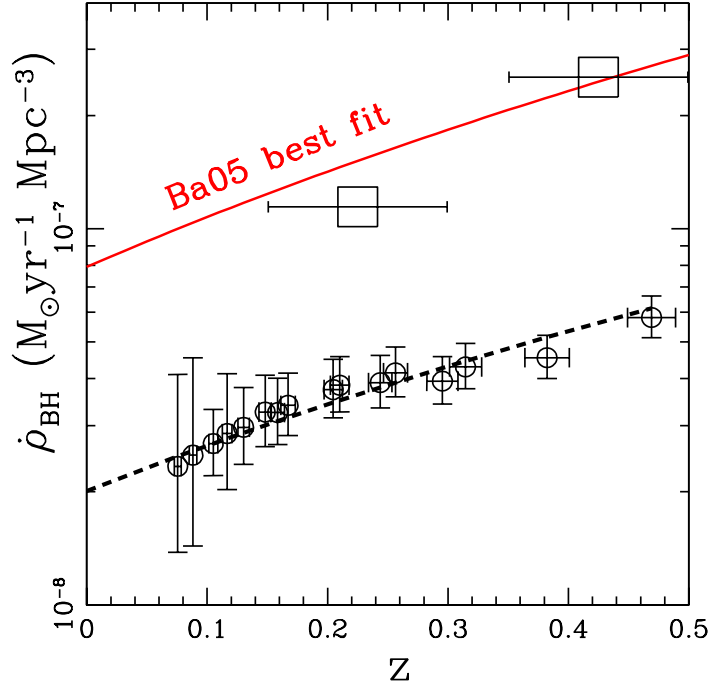


FIG. 15.— Comoving SMBH accretion rate density as a function of redshift for the AGES early-type galaxies. Because we are dealing with normal galaxies rather than X-ray bright AGNs, our results lie roughly a factor of four below the Ba05 data (open squares at $0.15 < z < 0.3$ and $0.35 < z < 0.5$) and the (solid) Ba05 best-fit curve (which is based on additional data out to $z \approx 1.2$). The slopes of the best-fit curves shown do agree to within errors, however. Our value is 2.9 ± 0.7 (dashed line), while Ba05 finds 3.2 ± 0.8 (for $z < 1.2$).

of the sample. Third, the Poisson and bootstrap error estimates are similar at all redshifts, which they would not be if a small number of individual, high-count sources (AGNs) were hidden within the sample. This disfavors small to moderate AGN contamination. Significant AGN contamination is also disfavored by our analysis and comparisons to previous work in Section 5.1.

5.1. Star Formation Rates in the Late-Type Galaxies

Studies of star formation over the redshift range $0 \lesssim z \lesssim 3$ have demonstrated that the relationship between X-ray luminosity and SFRs is reasonably universal (e.g., Brandt et al. 2001; Seibert et al. 2002; Nandra et al. 2002; Cohen 2003; Grimm et al. 2003; Persic et al. 2004; Reddy & Steidel 2004; Lehmer et al. 2005). We use Eqn. (1) to estimate the hard band SFR from $L_{\text{x,hard}}^{\text{HMXB}} = L_{\text{x,hard}}^{\text{LATE}} - L_{\text{x,hard}}^{\text{LMXB}}$, where $L_{\text{x,hard}}^{\text{LMXB}}$ is based on Eqn. (2) and a typical LMXB spectrum with $HR = 0$ (e.g., Munoz et al. 2004) and $L_{\text{x,hard}}^{\text{LATE}}$ is given in Eqn. (15). The result is

$$\text{SFR}_{\text{hard}} = (6.4 \pm 1.8) \langle L_{\text{K}} / L_{\text{K}^*} \rangle^{1.2 \pm 0.4} \times (1+z)^{3.4 \pm 1.2} M_{\odot} \text{yr}^{-1}. \quad (19)$$

Using Eqn. (3) to estimate the stellar mass M_* of the galaxies, we find that SFR_{hard} corresponds to a specific star formation rate ($\text{SSFR} = \text{SFR} / M_*$) of

$$\text{SSFR}_{\text{hard}} = (8.4 \pm 2.4) \times 10^{-2} (1+z)^{3.4 \pm 1.2}$$

$$\times \langle M_*/10^{11} M_\odot \rangle^{0.2 \pm 0.4} \text{Gyr}^{-1}. \quad (20)$$

Based on the work of Ranalli et al. (2003, as modified by Gilfanov et al. 2004) we also use Eqn. (1) to estimate the soft band SFR from $L_{x,\text{soft}}^{\text{HMXB}} = L_{x,\text{soft}}^{\text{LATE}} - L_{x,\text{soft}}^{\text{LMXB}}$:

$$\text{SFR}_{\text{soft}} = (3.4 \pm 0.7) \langle L_K/L_{K*} \rangle^{1.1 \pm 0.2} \times (1+z)^{2.4 \pm 1.0} M_\odot \text{yr}^{-1} \quad (21)$$

and a corresponding specific star formation rate of

$$\text{SSFR}_{\text{soft}} = (4.3 \pm 0.9) \times 10^{-2} (1+z)^{2.4 \pm 1.0} \times \langle M_*/10^{11} M_\odot \rangle^{0.1 \pm 0.2} \text{Gyr}^{-1}. \quad (22)$$

As shown in Figure 12, the results of earlier SSFR studies by Bauer et al. (2005), Bell et al. (2005), and Feulner et al. (2004) fall within the range encompassed by our hard and soft band SSFR trends (Eqns. 20 and 22), but we have smaller uncertainties due to our larger sample size. Our results also agree with those of more recent analyses of comparably large galaxy samples (Noeske et al. 2007 and Zheng et al. 2007) in bins of similar stellar mass ($10.5 \lesssim \log(M_*/M_\odot) \lesssim 11$) and redshift ($0.2 \lesssim z \lesssim 0.45$ and $z \simeq 0.3$, respectively).

We compute the star formation rate per comoving volume, $\dot{\rho}_*$, by integrating Eqns. (19) and (21) over the comoving density of the late-type galaxies (see Section 2.2). These results are shown in Figure 13. We find

$$\dot{\rho}_{*,\text{hard}} = (2.1 \pm 0.4) \times 10^{-2} (1+z)^{2.9 \pm 0.7} \frac{M_\odot}{\text{yr Mpc}^3} \quad (23)$$

and

$$\dot{\rho}_{*,\text{soft}} = (1.6 \pm 0.3) \times 10^{-2} (1+z)^{2.5 \pm 0.5} \frac{M_\odot}{\text{yr Mpc}^3}, \quad (24)$$

for the hard and soft bands respectively. As illustrated in Figure 13, our results are broadly consistent with the range of $\dot{\rho}_*$ values inferred from the standard extinction-corrected ultraviolet luminosity measurements of GALEX (Schiminovich et al. 2005).

It is important to note that significantly larger extinction corrections have already been ruled out by neutrino detectors. Values of $\dot{\rho}_*$ more than 50% larger than $\dot{\rho}_{*,\text{hard}}$ would be in serious conflict with the Super-Kamiokande upper limit (Malek et al. 2003) on the Diffuse Supernova Neutrino Background (DSNB) from $M > 8M_\odot$ stars (Strigari et al. 2005, Hopkins and Beacom 2006).

Our soft-band estimates of $\dot{\rho}_*$ sit closer to the GALEX minimum extinction correction curve. Nevertheless, the consistency of our hard and soft band results with each other and with the range of GALEX results indicates that we are in general agreement with earlier studies (e.g., based on H α measurements: Tresse & Maddox 1998, Tresse et al. 2002, Pérez-González et al. 2003, and Brinchmann et al. 2004 and the meta-analysis of Hogg 2001) as well as more recent comprehensive studies (e.g., Hopkins & Beacom 2006).

The level of agreement between our hard and soft band results also provides a check on the contamination of our sample by AGNs. We first note that the soft band SSFR

and $\dot{\rho}_*$ values (Eqns. 22 and 24) are systematically lower than the corresponding hard band values (Eqns. 20 and 23), but this is not uncommon. Many previous studies have also generally inferred lower SFR and $\dot{\rho}_*$ values based on soft band flux (e.g., G03 and Norman et al. 2004), suggesting that a low-normalization conversion between the soft band X-ray flux and the star formation rate (e.g., Hornschemeier et al. 2005), rather than contamination in the hard band, is to blame for this discrepancy. Furthermore, if sources harder than X-ray binaries, like Type II AGNs (see Figure 7), were contributing excess hard band emission to the late-type galaxy flux, $\dot{\rho}_{*,\text{hard}}$ (Eqn. 23) would lie above rather than slightly below the GALEX best-fit curve (Figure 13).

5.2. Accretion Rates in the Early-Type Galaxies

For the early-type galaxies, we use Eqn. (2) to estimate and subtract the contamination from LMXBs and use the remaining hard X-ray luminosity to determine the average supermassive black hole growth rate via Eqn. (4). Assuming a constant accretion efficiency of $\epsilon = 0.1$, we find that

$$\dot{M}_{\text{BH}} = (5.8 \pm 1.1) \times 10^{-6} \langle L_K/L_{K*} \rangle^{1.1 \pm 0.4} \times (1+z)^{3.3 \pm 0.7} M_\odot \text{yr}^{-1}. \quad (25)$$

This growth rate (see Figure 14) is roughly an order of magnitude below the estimates of Ba01 ($\dot{M}_{\text{BH}}^{\text{B01}} \gtrsim 10^{-4} M_\odot \text{yr}^{-1}$), because we are considering very different source populations. The Ba01 estimates are based on directly detected X-ray sources with luminosities exceeding 10^{42} erg s $^{-1}$, while we have eliminated such bright sources and consider only “normal” galaxies with mean luminosities of order 10^{41} erg s $^{-1}$. The rapid redshift evolution of the accretion rate in normal galaxies is consistent, however, with the redshift evolution of bright AGNs found by Ba01 and Ba05.

We estimate the accretion rate density $\dot{\rho}_{\text{BH}}$ by integrating the accretion rate per unit (stellar) luminosity over the early-type galaxy luminosity function (see Section 2.2). We find that

$$\dot{\rho}_{\text{BH}} = (2.0 \pm 0.4) \times 10^{-8} (1+z)^{2.9 \pm 0.7} M_\odot \text{yr}^{-1} \text{Mpc}^{-3}. \quad (26)$$

As shown in Figure 15, the evolution rate we determine is consistent with the rates found by Ba01 ($\dot{\rho}_{\text{BH}} \propto (1+z)^{3 \pm 1}$) and Ba05 ($\dot{\rho}_{\text{BH}} \propto (1+z)^{3.2 \pm 0.8}$) but we have a systematically lower normalization for $\dot{\rho}_{\text{BH}}$ because of the different source populations we have examined. This suggests that even at $z \lesssim 0.5$ the aggregate growth rate of black holes in normal galaxies is still a factor of a few less than that occurring in the much smaller number of bright, low-redshift AGNs.

6. SUMMARY AND CONCLUSIONS

After eliminating AGNs flagged by AGES spectroscopy and X-ray sources brighter than our luminosity limit (Eqn. 8), we used a stacking technique to determine the average X-ray properties of a magnitude-limited sample of 6146 ($R < 20$ mag, $z < 0.6$) apparently normal galaxies. The results substantially improve our knowledge of normal

galaxy X-ray evolution over the redshift range $0.1 \lesssim z \lesssim 0.5$, which has been difficult to probe based on either local studies of individual objects or small-area deep fields.

We spectroscopically divided the galaxies into late-type and early-type subsamples. The spectroscopic signatures of star formation, spatially extended radial emission profiles, luminosity evolution, and low LMXB emission ($\lesssim 15\%$) of the late-type galaxies suggest that their X-ray emission is dominated by HMXBs and therefore traces the star formation rate.

Conversely, because the early-type galaxies lack spectroscopic evidence for star formation, yet have rapidly evolving hard X-ray luminosities that are well in excess of that expected from LMXBs ($\lesssim 20\%$), we concluded that their emission is increasingly dominated by AGNs at higher redshifts.

When we use a double power law ($L_x \propto L_K^\alpha (1+z)^\beta$, Eqn. 5) to fit the trends in the X-ray emission, we see that the X-ray luminosity increases monotonically from low mass galaxies at low redshift to high mass galaxies at high redshift for both galaxy types. The redshift evolution of the late-type galaxies, $L_x \propto (1+z)^{3\pm 1}$, is in good agreement with previous estimates (e.g., H02, Ptak et al. 2001) and with theoretical expectations for normal, star-forming galaxies (Ghosh & White 2001). The optical luminosity dependence of the late-type galaxy emission, roughly $L_x \propto L_K^{1.2\pm 0.3}$, also matches previous results (e.g., S01; David, Jones, & Forman 1992). In addition, the specific star formation rates, $\text{SSFR} = \text{SFR}/M_*$, and star formation rate densities, $\dot{\rho}_*$, we infer from the hard and soft band emission of the late-type galaxies span the range of previously reported values (Figures 12 and 13).

The specific X-ray luminosities we found for the early-type galaxies are in good agreement with the results of past studies (O’Sullivan et al. 2001, G03, B05, and Lehmer et al. 2007). Additionally, our work provides the first X-ray estimates of the SMBH accretion rates, \dot{M}_{BH} , and accretion rate densities, $\dot{\rho}_{\text{BH}}$, in normal galaxies at these redshifts. Our findings suggest that the redshift evolution of low luminosity AGNs in our early-type galaxy sample is similar to that of higher luminosity AGNs (Ba01 and Ba05), which we exclude from our analysis. However, the lower luminosity AGNs contribute little to the overall growth of supermassive black holes. In general, our work shows that there is a continuum rather than a sudden break in the star formation and SMBH accretion histories of galaxies from the powerful starbursts and AGNs of the past to the fainter, optically-normal galaxies more prevalent today.

Our analysis of the X-ray evolution of galaxies in the NDWFS XBoötes field can be significantly expanded in the future. A second phase of AGES has doubled the size of the spectroscopic sample and extended the redshift range of galaxies. If combined with photometric redshifts based on the very extensive, multiwavelength NDWFS photometry, it will be possible to reach $z \sim 1$ to a uniform luminosity limit and greatly reduce statistical errors.

C.R.W. thanks John Beacom, Mark Brodwin, Xinyu Dai, Stephan Frank, Oleg Gnedin, Andy Gould, Dirk Grupe, Himel Ghosh, Matt Kistler, Smita Mathur, Pat Osmer, Rick Pogge, Ken Rines, Louie Strigari, Ezequiel Treister,

Meg Urry, Pieter van Dokkum, Jeff van Duyne, David Weinberg, Jong-Hak Woo and Hasan Yuksel for helpful discussions. We also thank the referee for useful and extensive comments.

This research was supported by the National Optical Astronomy Observatory which is operated by the Association of Universities for Research in Astronomy (AURA), Inc. under a cooperative agreement with the National Science Foundation. Spectroscopic observations reported here were obtained at the MMT Observatory, a joint facility of the Smithsonian Institution and the University of Arizona. We thank the CXC for scheduling the *Chandra X-ray Observatory* observations that made this work possible and the CXC Data Processing Team for the pipeline data.

REFERENCES

- Barger, A. J., et al. 2001, *AJ*, 122, 2177 (Ba01)
 Barger, A. J., et al. 2005, *AJ*, 129, 578 (Ba05)
 Bauer, F. E., Alexander, D. M., Brandt, W. N., Hornschemeier A. E., Vignali, C., Garmire, G. P., Schneider D. P. 2002, *ApJ*, 568, L85
 Bauer, A. E., et al. 2005, *ApJL*, 625, 89
 Becker, R. H., White, R. L., & Helfand, D. J. 1995, *ApJ*, 450, 559
 Bell, E. F., 2004, Invited Review in “Planets to Cosmology: Essential Science in Hubble’s Final Years”, Ed. M. Livio (Cambridge: CUP), astro-ph/0408023
 Bell, E. F., et al. 2005, *ApJ*, 625, 23
AJ, 121, 2538
 Blanton, M. J., et al. 2003, *AJ*, 125, 2348
 Brand, K., et al. 2005, *ApJ*, 626, 723 (B05)
 Brandt, W. N., et al. 2001, *AJ*, 122, 2810
 Brinchmann J. & Ellis, R. S. 2000, *ApJ*, 536, L77
 Brinchmann J., et al. 2004, *MNRAS*, 351, 1151
 Brown, Warren R., Geller, Margaret J., Fabricant, Daniel G., & Kurtz, Michael J. 2001 *AJ*, 122, 714
 Civano, Francesca, Comastri, Andrea, Brusa, Marcella 2005, *MNRAS*, 358, 693
 Cohen, Judith G., 2003, *ApJ*, 598, 288
 Colbert, Edward J. M., et al. 2004, *ApJ*, 602, 231
 Cowie, L. L., et al. 1996, *AJ*, 112, 839
 Cowie, L. L., et al. 2003, *ApJ*, 584, L57
 David, L. P., Jones, C., & Forman, W. 1992, *ApJ*, 388, 82
 De Luca, A. & Molendi, S. 2004, *A&A*, 419, 837
 de Vries, W. H., Morganti, R., Röttgering, H. J. A., Vermeulen, R., van Breugel, W., Rengelink, R., & Jarvis, M. J. 2002, *AJ*, 123, 1784
 Dunlop, J. S., et al. 2003, *MNRAS*, 340, 1095
 Eisenhardt, P. R., et al., 2004, *ApJS*, 154, 48
 Elston, R. J., et al., 2006, *ApJ*, 639, 816
 Fabbiano, G. 1989, *ARA & A*, 27, 87
 Fabbiano, G. & White, N., 2003, in: *Compact Stellar X-ray Sources*, Cambridge University Press (eds., W. Lewin & M. van der Klis); (astro-ph/0307077)
 Fabricant, Daniel G., et al. 1998, *SPIE*, 3355, 285
 Fabricant, Daniel G., et al. 2005, *PASP* 117, 1411
 Ferreras, L., Pasquali, A., de Carvalho, R. R., de la Rosa, I. G., Lahav, O., 2006, *MNRAS*, 370, 828
 Feulner, Georg, et al. 2004, *MNRAS*, 358, 1
 Forman, W., Jones, C., & Tucker, W. 1994, *ApJ*, 429, 77
 Formigini, L. & Brosch, N. 2004, *MNRAS*, 350, 1067
 Franceschini, A. et al. 2005, *ApJ*, 129, 2074
 Georgakakis, A., et al. 2003, *MNRAS*, 344, 161 (G03)
 Georgakakis, A., et al. 2007, *MNRAS*, 377, 203
 Ghosh, P. & White, N. E. 2001, *ApJ*, 559, 97
 Gilfanov, M., Grimm, H.-J., Sunyaev, R. 2004 *MNRAS*, 347, L57
 Gilfanov, M. 2004 *MNRAS*, 349, 146
 Grimm, H.-J. et al. 2003, *MNRAS*, 339, 793
 Guzman, R., et al. 1997, *ApJ*, 489, 559
 Hasinger, G. 2004, “Growing black holes: accretion in a cosmological context”, Eds. A. Merloni, S. Nayakshin, & R. A. Sunyaev (Berlin: Springer), astro-ph/0412576
 Hasinger, Günther, Miyaji, Takamitsu, & Schmidt Maarten 2005, *A&A*, 441, 417
 Hogg, D. W. 2001, *PASP*, arXiv:astro-ph/0105280, submitted
 Hoopes, C. G. 2004, American Astronomical Society Meeting, 204
 Hopkins, A. M. & Beacom, J. F., 2006, *ApJ*, 651, 142
 Hopkins, P. F., et al., 2007, *ApJ*, 654, 731

- Hornschemeier, A. E. et al., 2002, *ApJ*, 568, 82 (H02)
- Hornschemeier, A. E. et al. 2005, *AJ*, 129, 86
- Jannuzi, B. T. & Dey, A. 1999, in "Photometric Redshifts and the Detection of High Redshift Galaxies", ASP Conference Series, Vol. 191, Edited by R. Weymann, L. Storrie-Lombardi, M. Sawicki, & R. Brunner., 111
- Juneau, Stéphanie, et al. 2005, *ApJ*, 619, L135
- Kenter, A. T., et al., 2005, *ApJS*, 161, 9
- Kim, Dong-Woo & Fabbiano, G., 2004, *ApJ*, 611, 846
- Kim, E., et al. 2006, *ApJ*, 647, 276
- Kochanek, C. S., et al. 2001, *ApJ*, 560, L566
- Laird, E. S., et al. 2005, *MNRAS*, 359, 47
- Laird, E. S., et al. 2006, *MNRAS*, 373, 217
- Lehmer, B. D., et al. 2005, *AJ*, 121, 1
- Lehmer, B. D., et al. 2007, *ApJ*, 657, 681
- Lehmer, B. D., et al. 2008, *ApJ*, 681, 1163
- Malek, M., et al. 2003, *Phys. Rev. Lett.*, 90, 061101
- Mathews, W. G. & Brighenti, F., 2003, *ARA&A*, 41, 191
- McLeod, K. K. & McLeod, B. A. 2001, *ApJ*, 546, 782
- Miyaji, Takamitsu 2004, Multiwavelength AGN Surveys, Proc. Guillermo Haro Conference, Eds. Ral Mújica & Roberto Maiolino (World Scientific, Singapore), astro-ph/0403466
- Muno, M. P., et al. 2004, *ApJ*, 613, 1179
- Murray, S., et al. 2005, *ApJS*, 161, 1 (astro-ph/0504084)
- Nandra, K., Mushotzky, R. F., Arnaud, K., Steidel, C. C., Adelberger, K. L., Gardner J. P., Teplitz, H. I., Windhorst, R. A. 2002, *ApJ*, 576, 625
- Nandra K. et al., 2004, *MNRAS*, 356, 568
- Noeske, K. G. et al., 2007, *ApJ*, 660, 47
- Norman, Colin et al., 2004, *ApJ*, 607, 721
- O'Sullivan, Ewan, Forbes, Duncan A., Ponman, Trevor J. 2001, *MNRAS*, 328, 461 (OS01)
- Pérez-González, P. G., et al. 2003, *ApJ*, 591, 827
- Pérez-González, P. G., et al. 2005, *ApJ*, 630, 82
- Persic, M. et al., 2004, *A&A*, 420, 79
- Ptak, A., et al. 1999, *ApJS*, 120, 179
- Ptak, A., et al. 2001, *ApJ*, 559, L91
- Ptak, A., et al. 2007, *ApJ*, 667, 826
- Ranalli, P., et al. 2003, *A & A*, 399, 39
- Reddy, Naveen & Steidel, Charles C. 2004, *ApJ*, 603, L13
- Roll, John B., et al. 1998, *SPIE*, 3355, 324
- Rosati, P., et al. 2002, *ApJ*, 566, 667
- Schiminovich, D., et al. 2005, *ApJ*, 619, 47
- Seibert, Mark, Heckman, Timothy M., Meurer, Gerhard R. 2002, *AJ*, 124, 46
- Shankar, F., et al. 2004, *MNRAS*, 354, 1020
- Shapley, Alice, Fabbiano, G., Eskridge, P. B. 2001, *ApJS*, 137, 139 (S01)
- Smith, David A. & Wilson, Andrew S. 2003, *ApJ*, 591, 138
- Stark, A. A., et al. 1992, *ApJS*, 79, 77
- Strickland, D. K., et al. 2004, *ApJS*, 151, 193
- Strigari, L. E., Beacom J. F., Walker, T. P., & Zhang P., 2005, *Journal of Cosmology & Astro-Particle Physics*, 4, 17
- Tozzi P. et al., 2001, *ApJ*, 562, 42
- Tresse, L., & Maddox, S. J., 1998 *ApJ*, 495, 691
- Tresse, L., et al. 2002 *MNRAS* 337, 369
- Tzanavaris, P. & Georgantopoulos, I. 2008, *A & A*, 480, 663
- Ueda, Y., et al. 2003, *ApJ*, 598, 886
- Wang, Q. D., et al. 1999, *ApJ*, 523, 121
- Zheng, X. Z., et al. 2007, *ApJ*, 661, 41